JCI The Journal of Clinical Investigation

dmPFC-vlPAG projection neurons contribute to pain maintenance thresholds and anxiolytic behaviors

Jun-Bin Yin, … , Yu-Lin Dong, Yun-Qing Li

J Clin Invest. 2020. https://doi.org/10.1172/JCI127607.

Research In-Press Preview Neuroscience

Graphical abstract

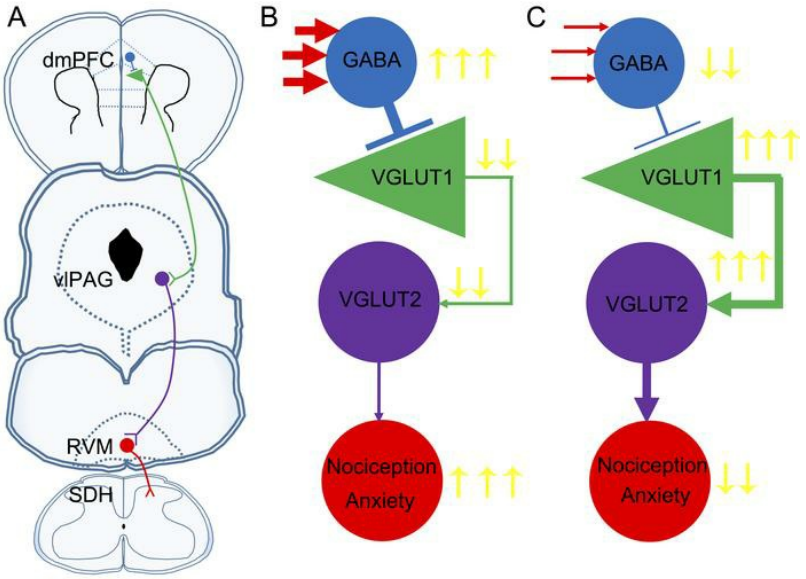

dmPFC-vlPAG projection neurons contribute to pain maintenance thresholds and anxiolytic behaviors

Jun-Bin Yin[1,2,3,4#], Shao-Hua Liang[1,5#], Fei Li[1,6#], Wen-Jun Zhao[1,6], Yang Bai[1,3], Yi Sun[1,5,3], Zhen-Yu Wu[1,3], Tan Ding[7], Yan Sun[6], Hai-Xia Liu[1], Ya-Cheng Lu[1], Ting Zhang[1], Jing Huang[1], Tao Chen[1], Hui Li[1,3], Zhou-Feng Chen[3], Jing Cao[8], Rui Ren[4],Ya-Nan Peng[4], Juan Yang[4], Wei-Dong Zang[8], Xiang Li[9*], Yu-Lin Dong[1*], Yun-Qing Li[1,4,8*]

[1]*Department of Anatomy, Histology and Embryology and K. K. Leung Brain Research Centre, The Fourth Military Medical University, Xi'an 710032, China*

[2]*Department of Neurology, the 960th Hospital of PLA, Jinan 250031, China*

[3]*Center for the Study of Itch, Washington University School of Medicine, St. Louis, MO 63110, U.S.A*

[4]*Key Laboratory of Brain Science Research & Transformation in Tropical Environment of Hainan Province, Haikou 571199, China*

[5]*Department of Human Anatomy, Binzhou Medical Colleage, Yantai 264000, China*

[6]*Cadet Brigade, the Fourth Military Medical University, Xi'an 710032, PR China*

[7]*Department of Orthopedics, Xijing Hospital, the Fourth Military Medical University, Xi'an 710032, PR China*

[8]*Department of Anatomy, Basic Medical College, Zhengzhou University, Zhengzhou 450001, China*

[9]*Department of Orthopaedics, The First Affiliated Hospital with Nanjing Medical University, Nanjing 210029, China*

Conflict of Interest: The authors have declared that no conflict of interest exists.

#These authors contributed equally to this work.

*Address correspondence to: Yun-Qing Li or Yu-Lin Dong, Department of Anatomy, Histology and Embryology and K. K. Leung Brain Research Centre, The Fourth Military Medical University, No. 169 Changle West Road, Xi'an 710032, China. Phone: 86-29-84772706; Email: deptanat@fmmu.edu.cn (Y-Q Li); donganat@fmmu.edu.cn (Y-L Dong). Or to Xiang Li, Department of Orthopaedics, The First Affiliated Hospital with Nanjing Medical University, No. 300 Nanjing Road, 210029, China. Phone: 86-25-68303194; Email: lixiangjsph@163.com (X Li).

Abstract

The dorsal medial prefrontal cortex (dmPFC) has been recognized as a key cortical area for nociceptive modulation. However, the underlying neural pathway and the function of specific cell types remain largely unclear. Here, we showed that lesions of the dmPFC induced an algesic and anxious state. By using multiple tracing methods including rabies-based transsynaptic tracing method, an excitatory descending neural pathway from the dmPFC to the ventrolateral periaqueductal gray (vlPAG) was outlined. Specific activation of the dmPFC-vlPAG neural pathway by an optogenetic manipulation, produced analgesic and anxiolytic effects in a chronic pain mice model. Inhibitory neurons in the dmPFC were specifically activated by using a chemogenetic approach, which logically produced an algesic and anxious state under both normal and chronic pain conditions. Antagonists of $GABA_AR$ or mGluR1 were applied to the dmPFC, which produced analgesic and anxiolytic effects. In summary, the present results suggest that the dmPFC-vlPAG neural pathway might participate in the maintenance of pain thresholds and anxiolytic behaviors under normal conditions, while silencing or suppressing the dmPFC-vlPAG pathway might be involved in the initial stages and maintenance of chronic pain and the emergence of anxiety-like behaviors.

Key words： dmPFC; vlPAG; chronic pain; negative emotion; neural pathway; optogenetic approach; chemogenetic approach; inhibitory interneuron

Introduction

Patients with chronic pain usually suffer from not only severe pain perception but also negative emotions and decreased cognitive abilities (1, 2). Intractable and permanent pain conditions easily developed into a 'chronic pain cycle': chronic pain induces negative emotions including anxiety and depression, sleep disorder, and reduced activity and also affects the cognitive abilities (2-4). Conversely, negative emotions and reduced cognitive abilities further worsen chronic pain (5, 6). This 'chronic pain cycle' has made it very difficult to treat chronic pain clinically. There might be a special neural circuit that mediates this vicious cycle, which would be a good target for the treatment of chronic pain. Many studies have focused on the emotional components of pain, in an attempt to identify the neural pathway related to emotional pain (7-10). However, the underlying mechanisms for this 'chronic pain cycle' are still unclear.

One of useful ways, to address this 'chronic pain cycle', is to identify a special region or area in the cerebral cortex that is involved in the modulation of pain, emotions, and cognition. The dorsal medial prefrontal cortex (dmPFC), including the rostral anterior cingulate cortex (rACC) and prelimbic cortex (PL), is a region or area involved in all of these processes (11-13). Many previous studies have demonstrated that the functional deactivation of the dmPFC induced negative emotions and decreased cognitive abilities (14, 15). A few studies have also suggested that the deactivation of the dmPFC enhanced pain perception (8, 10, 16). Functional and morphological abnormalities in the dmPFC have been documented in a chronic pain animal model (17, 18). Both background and evoked activity of dmPFC neurons was decreased in an arthritis-induced chronic pain model (19, 20). It has been speculated that the progression of pain from an acute to a chronic state is accompanied by a decrease in dmPFC activity (21, 22). This pain-related inhibition of dmPFC neurons in the arthritic model depended on metabotropic glutamate receptor 1 (mGluR1)-mediated endogenous activation of gamma-aminobutyric acid receptor subtype A ($GABA_AR$) (19). However, the exact neural pathway from the dmPFC involved in pain modulation has only begun to be revealed (23). The periaqueductal gray (PAG)-rostral ventromedial medulla (RVM)-

spinal dorsal horn (SDH) pathway is one of the most important neural pathways involved in descending pain modulation (24-26). It has been demonstrated that specific activation of the vesicular glutamate transporter 2-immunoreactive (VGLUT2-ir) neurons in the ventrolateral subregion of the PAG (vlPAG), the region of the PAG that has been most closely linked to pain descending modulation, produced clear analgesic effects, which indicated that VGLUT2-ir neurons in the vlPAG are key relay points for descending pain modulation (27, 28). We hypothesized that dmPFC neurons project to the vlPAG and participate in descending pain modulation, based on the abundant projections from the superior nucleus in the frontal cortex to the vlPAG. Thus, the deactivation of the dmPFC-vlPAG neural pathway would induce the 'chronic pain cycle' and lead to increased suffering of patients with chronic pain.

To test whether this hypothesis is correct, chemical lesion, optogenetic, chemogenetic, molecular biological and behavioral pharmacological approaches were applied to demonstrate the involvement of the descending dmPFC-vlPAG pathway in pain modulation and negative emotion processing. In the present study, as a first step, many kinds of morphological approaches were used to establish the dmPFC-vlPAG neural pathway and investigate the chemical properties of the projection neurons. Functional investigations were also carried out to examine whether the dmPFC-vlPAG neural pathway is involved in pain-related and anxiety-like behaviors. Finally, different methods were used within the dmPFC to reveal the underlying molecular mechanisms related to this descending modulation of pain.

Results

Bilateral dmPFC lesions promote nociception under normal and chronic pain conditions.

To check whether the dmPFC participates in pain perception, kainic acid (KA) was injected into the bilateral dmPFC for damaging cells. The mechanical thresholds of mice in the normal and chronic pain conditions, after the KA injection, were evaluated (Figure 1A, B). Reduced densities and disordered arrangements of cells were observed

in the dmPFC following the KA injection (Figure 1C). The loss of neuronal cell bodies and proliferation of astrocytes were also indicators of dmPFC lesion (Supplementary Figure 1). Under normal condition, the dmPFC lesion significantly reduced the mechanical thresholds of both hindpaws (Figure 1D), and the mice showed obvious mechanical hyperalgesia. After the common peroneal nerve ligation (CPNL) model was established, bilateral dmPFC lesions significantly facilitated CPNL-induced hyperalgesia (Fig 1E F). However, the dmPFC lesion had no influence on the responses to nonnoxious mechanical stimulation (Figure 1G), which indicates that dmPFC lesions in naïve mice did not induce allodynia. The responses to nonnoxious stimuli of both hindpaws in the lesion group were significantly higher than those in the saline group (Fig 1H, I).

Bilateral dmPFC lesions induce anxiety-like behaviors

Chronic pain is often accompanied by anxiety-like behaviors. Therefore, the effects of the dmPFC lesion on the animals' anxiety-like behaviors induced by CPNL were assessed. CPNL mice exhibited a decreased percentage of time in the central area of the open field (OF) test at post-CPNL 14 days; in contrast, the total distance traveled in the OF was unaffected (Figure 1J-L). However, the dmPFC lesion significantly decreased the total distance traveled in the OF test (Figure 1J, K). What is interesting, CPNL would not induce more anxiety-like behaviors in the OF test after the dmPFC lesion (Figure 1K, L). Then, we further tested the effects of the dmPFC lesion on anxiety-like behaviors induced by CPNL in the elevated plus maze (EPM) test. CPNL decreased both the percentage of time spent in the open arms and percentage of entries into the open arms in the EPM (Figure 1J, M, and N). Similarly, after the dmPFC lesions, the CPNL mice didn't show more anxiety-like behaviors in the EPM test (Figure 1M, N). All these results indicate that CPNL-induced anxiety-like behaviors were not observed after neurons were damaged in the dmPFC. Although we have not investigated the underlying mechanism, the possible explanation for this result was the floor effect.

Projections from the dmPFC terminate onto the VGLUT2-ir neurons within the vlPAG

Given the important roles of the dmPFC in the modulations of nociception and anxiety-

like behaviors, it was critical to investigate the direct connections between the dmPFC and the vlPAG, which is known to play an important role in pain modulation. Fluoro-Gold (FG) was injected into the vlPAG. Many FG-labeled projection neurons were observed in the dmPFC, which also exhibited CaMKII immunoreactivity and expressed VGLUT1 mRNA (Supplementary Figure 2 and 3). Moreover, the FG-labeled neurons did not express both VGLUT2 mRNA and GAD67. The double staining of NeuN and FG showed that the projection neurons were mainly distributed in layers V and VI in the dmPFC (Figure 2A-D). These results indicated that there were direct innervations from the dmPFC excitatory pyramidal neurons to the vlPAG. To identify the synaptic connections, we applied a rabies-based, retrograde, transsynaptic tracing approach to identify the dmPFC monosynaptic inputs onto VGLUT2-ergic neurons in the vlPAG based on a transgenic mouse line expressing Cre recombinase in these neurons (Figure 2E-H). The starter neurons (GFP and dsRed double staining neurons) were localized in the vlPAG (Figure 2I-L). In the sections of the forebrain, many dsRed trans-synaptic labeled pyramidal projection neurons were observed in the dmPFC and anterior cingulate cortex (ACC) (Figure 2M-P). The above retrograde tracing results suggested that the excitatory pyramidal neurons in the dmPFC project to the VGLUT2-ir neurons in the vlPAG.

Consistent with the retrograde tracing investigation (Figure 3A), the anterograde tracer biotinylated dextran amine (BDA) was injected into the dmPFC and dense BDA-labeled fibers and terminals were observed in the vlPAG (Supplementary Figure 4). For further confirmation, AAV2/2-CaMKIIα-EYFP was injected into the dmPFC to infect the excitatory pyramidal neurons (Figure 3B, C). After 3 weeks, FG was injected into the RVM. Many EYFP-labeled fibers and terminals were observed in the vlPAG (Figure 3D). By using fluorescence *in situ* hybridization, the FG-labeled RVM projection neurons in the vlPAG were found, and most of them expressed VGLUT2 mRNA (Figure 3E-H). Moreover, the FG-labeled SDH projection neurons in the RVM expressing 5-HT can receive many VGLUT2-ir contacts (Supplementary Figure 5 and 6). To confirm the links of dmPFC and the PAG- rostroventral medulla (RVM) descending pain modulation system, AAV2/2-CaMKIIα-EYFP was injected into the

dmPFC and FG was injected into the RVM. FG-labeled RVM projection neurons in the vlPAG received the EYFP-labeled fiber contacts, which co-localized with the presynaptic marker Synapsin (Figure 3I-L). We also applied an anterograde transsynaptic tracing approach, following previous studies (29, 30), to identify the dmPFC monosynaptic inputs onto FG-labeled RVM projection neurons in the vlPAG (Figure 3M-P, Table S1). Again, these tracing studies indicated that there exists a descending pain modulation pathway-the dmPFC-vlPAG-RVM pathway.

Hypoactivity in dmPFC-vlPAG projection neurons of CPNL mice

To examine how CPNL affects neuronal activity of dmPFC-vlPAG projection neurons, we performed whole cell patch-clamp recordings from dmPFC-vlPAG projection neurons of control and CPNL mice (Figure 4A-F). Excitability of dmPFC-vlPAG projection neurons was decreased in CPNL mice group (Figure 4G, H). Importantly, the $GABA_AR$ blocker bicuculline (20 μM) reversed the low activity in dmPFC-vlPAG projection neurons, indicating that the observed CPNL-induced reduction in dmPFC-vlPAG projection neurons activity is mediated by enhanced GABAergic inputs (Figure 4G, H). Altogether, these data indicate that CPNL triggers a long-term $GABA_AR$-mediated inhibition in the dmPFC-vlPAG projection neurons.

Analgesic and anxiolytic effects of specifically activating the dmPFC-vlPAG neural pathway

Based on the hypoactivity in dmPFC-vlPAG pathway induced by CPNL, we became very interested in the role of the dmPFC-vlPAG neural pathway in pain modulation and pain-related anxiety-like behaviors. After specifically activating the dmPFC-vlAPG pathway by using optogenetic approach, the mechanical thresholds of the bilateral hindpaws were tested at 7 days post CPNL, and the behaviors in the open field (OF) and elevated plus maze (EPM) tests were also assessed at 14 days post CPNL (Figure 5A, B). After light stimulated, more neurons expressing Fos-ir around the EYFP fibers in the vlPAG were observed (Figure 5C-F). This indicates that the neurons in the vlPAG were activated by stimulating the fibers coming from the dmPFC. Obvious analgesic effects were observed on the not only ipsilateral but also contralateral hindpaw in the CPNL mice, following dmPFC-vlPAG pathway specifically activated (Figure 5G).

While, in the CPNL mice infected with AAV2/2-CaMKIIα-EYFP, the light stimulation had no effects on the mechanical thresholds. Unexpected, the activation of dmPFC-vlPAG pathway had no obvious effects on both the total distance traveled and the percentage of time spent in the central area in the OF test at 14 days post CPNL (Figure 5H, I). However, both the reduced percentage of time spent in (Figure 5J) and percentage of entries into (Figure 5K) the open arms in the EPM test were significantly reversed during blue light stimulation in the mice that received the hChR2-EYFP virus injection. These optogenetic results suggest that specific activation of the dmPFC-vlPAG neural pathway produced analgesic and anxiolytic effects in the CPNL model. The dmPFC-vlPAG neural pathway was involved in the modulation of nociception and anxiety-like behaviors.

Specifically activating inhibitory neurons in the dmPFC facilitates nociception and anxiety-like behaviors

Activation of the local inhibitory neurons potentially suppressed pyramidal neurons within the dmPFC and resulted in deactivating the dmPFC-vlPAG pathway. The Designer Receptors Exclusively Activated by Designer Drugs (DREADDs) method was introduced to investigate the functional roles of the local inhibitory neurons in the dmPFC on the modulations of nociception and anxiety-like behaviors (Figure 6A, B). The triple labeling results showed that many GAD67-ir inhibitory neurons expressed mCitrin and Fos (Figure 6C-J), which indicate that the inhibitory neurons were certainly activated after the CNO *i.p.* injection. Under normal conditions, specific activation of inhibitory neurons in the dmPFC clearly reduced the mechanical thresholds of the bilateral hindpaws (Figure 6K, L). After CPNL was established, CNO *i.p.* injection further reduced the mechanical thresholds of the bilateral hindpaws in mice that received the hM3Dq-mCitrin injection (Figure 6K, L). The above results suggest that activation of inhibitory neurons in the dmPFC produced hyperalgesic states under both normal and chronic pain conditions.

Then, the effects of specific activation of local inhibitory neurons on anxiety-like behaviors in the OF and EPM under normal and chronic pain conditions were tested. Under normal conditions, both the total distance traveled (Figure 6M) and the

percentage of time in the central area (Figure 6N) in the OF test were significantly decreased by specifically activating inhibitory neurons in the dmPFC. In the EPM test, CNO injections also significantly suppressed the percentage of time in (Figure 6O) and the percentage of entries into (Figure 6P) the open arms for the mice that received hM3Dq-mCitrin virus injections. At 14 days after CPNL, the total distance traveled in the OF test was significantly reduced by specifically activating inhibitory neurons (Figure 6Q). And the percentage of time in the central area in the OF test was also clearly further suppressed (Figure 6R). In the EPM test, the CNO injection also significantly further suppressed the percentage of time in (Figure 6S) and the percentage of entries into (Figure 6T) the open arms in the mice that received the hM3Dq-mCitrin virus injection. It was indicated that the activation of inhibitory neurons in the dmPFC induced anxiety-like behaviors in the normal mice and even worsen chronic pain-induce anxiety-like behaviors.

Specifically activating inhibitory neurons in the dmPFC reverses activation of dmPFC-vlPAG pathway-induced analgesic and anxiolytic behaviors

Combined optogenetic and DREADDs methods were used to check the roles of local inhibitory interneurons on the dmPFC-vlPAG pathways. The detailed test procedures and different virus were presented in Figure 7A, B and Table S1. After the behavioral investigations, dmPFC-vlPAG projection neurons expressing hM3Dq-eGFP (green) and inhibitory neurons expressing hChR2-mCherry (red) could be observed in the dmPFC (Figure 7C). A separate group of animals was prepared for functional characterization of the hChR2 and hM3Dq. Blue light activation of the hChR2 in acute brain slices reliably elicited action potential spikes in inhibitory neurons following different stimulation frequency (Figure 7D). A bath application of 40 μM CNO induced a transient depolarization and robust action potential firing in dmPFC-vlPAG projection neurons (Figure 7E). When we recorded the projection neurons, light stimulation induced obvious inhibitory postsynaptic currents (IPSCs) (Figure 7F). Picrotoxin (PTX), the antagonist of GABAAR, completely blocked the light evoked IPSCs (Figure 7G). Seven days after CPNL was established, CNO *i.p.* injection significantly increased the mechanical thresholds of the ipsilateral hindpaw (Figure 7H). Specifically

activating inhibitory neurons by blue light stimulation reversed these analgesic effects. In the OF test, activation of neither projection neurons nor inhibitory neurons in the dmPFC affected the total distance (Figure 7I). At the same time, specifically activating inhibitory neurons worsen CPNL-induced reduction of the percentage of time in the central area (Figure 7J). However, in the EPM test, specifically activating inhibitory neurons significantly reversed activation of projection neurons-induced anxiolytic effects (Figure 7K, L). These results provide functional evidences that the local inhibitory neurons in the dmPFC innervate the projection neurons on the dmPFC-vlPAG pathway, and the activation of inhibitory neurons in the dmPFC induced anxiety-like behaviors and even worsen chronic pain-induce anxiety-like behaviors through the dmPFC-vlPAG descending pathway.

Both $GABA_AR$ and mGluR1 in the dmPFC are involved in chronic pain sensations and anxiety-like behaviors

The above results showed that lesions of the dmPFC or deactivation of the dmPFC-vlPAG neural pathway exacerbated mechanical hyperalgesia and anxiety-like behaviors in the CPNL model. However, the potential molecular mechanism remains unknown. Previous study has shown that $GABA_AR$ and mGluR1 in the dmPFC are involved in the deactivation of the dmPFC in an arthritis pain model (19). By using Western blot, significantly increased $GABA_AR$ and mGluR1 expression was observed in the dmPFC at 7 days post CPNL (Supplementary Figure 7). The mechanical thresholds and behaviors in the OF and EPM under normal and chronic pain conditions were tested by using behavioral pharmacologic approaches (Figure 8A, B). Many Fos-expressing neurons and the place of cannula in the dmPFC indicate that the specific antagonists of $GABA_AR$ and mGluR1 were reliably injected into the dmPFC and functionally activated some neurons (Figure 8C-E).

Under normal condition, the mechanical thresholds of the bilateral hindpaws were not changed by injecting bicuculline (0.1 μg) or LY367385 (specific mGluR1 antagonist, 0.4 nmol) into the dmPFC (Figure 8F, G). However, bicuculline or LY367385 injections into dmPFC produced obvious analgesic effects at 7 days post CPNL. There were no obvious differences in the mechanical thresholds between bicuculline group and

LY367385 group. Under normal conditions, bicuculline injection significantly increased the total distance traveled and the percentage of time spent in the central area in the OF test (Figure 8H, I). However, LY367385 injection had no obvious influence on those behaviors. While, bicuculline or LY367385 dmPFC injections had no influence on the percentage of time in and percentage of entries into the open arms in the EPM test (Figure 8J, K). At 14 days post CPNL, the total distance traveled and the percentage of time spent in the central area in the OF test were significantly increased by bicuculline injection into the dmPFC (Figure 8H, I). However, LY367385 injection only increased the percentage of time in the central area. In the EPM test, both the percentage of time in and percentage of entries into the open arms were significantly increased following bicuculline or LY367385 injections (Figure 8J, K). The above results indicate that the inhibition of $GABA_A$Rs or mGluR1s might be a useful approach to rescue hyperalgesia and anxiety-like behaviors under chronic pain condition.

Discussion

In the present study, we presented an excitatory 'Top-Down' neural pathway from dmPFC to vlPAG, which used glutamate as a neurotransmitter and acted on VGLUT2-containing neurons in the vlPAG. Under normal conditions, the dmPFC-vlPAG neural pathway plays important roles in maintaining the mechanical thresholds of the hindpaws and normal behavior in the open field (OF) and elevated plus maze (EPM) tests. The deactivation of the dmPFC-vlPAG neural pathway, by chemical lesions of dmPFC or specific activation of inhibitory neurons in the dmPFC, reduced the mechanical thresholds of hindpaws under both normal and chronic pain conditions and induced anxiety-like behaviors. Moreover, the activation of inhibitory neurons in the dmPFC even worsened the negative emotions under chronic pain conditions. Analgesic and anxiolytic effects were observed after activating the dmPFC-vlPAG neural pathway by using optogenetic approaches. By using behavioral pharmacological approaches, $GABA_A$R and mGluR1 in the dmPFC were shown to be involved in the initiation and maintenance of chronic pain and negative emotions. Based on the results of the present study, we speculated that the deactivation of the dmPFC-vlPAG neural pathway

initiated and maintained mechanical hyperalgesia and CPNL-induced anxiety-like behaviors under chronic pain conditions. Thus, these processes might be the underlying mechanism for the 'chronic pain cycle', which might be a potential target for the treatment of chronic pain in clinical practice.

GABAergic inhibitory interneurons were involved in the modulation of excitatory pyramidal neurons in the dmPFC (31, 32). Our present investigation showed that specific activation of pyramidal neurons in the dmPFC produced analgesic and anxiolytic effects. While, specific activation of inhibitory neurons in the dmPFC worsened CPNL-induced mechanical hyperalgesia and anxiety-like behaviors. Only lesions of the contralateral, not ipsilateral prelimbic cortex (PL), attenuated complete Freund's adjuvant (CFA)-induced anxiety-like behaviors and heat hyperalgesia (10), which was contradictory to our results that bilateral lesions of dmPFC worsened CPNL-induced mechanical hyperalgesia. Regarding this difference, we think that differential effects of the chemical drugs used in these two investigations (quinolinic acid *vs* kainic acid) on various lesioned neuron types can not be excluded. Different chronic pain models (CFA *vs* CPNL) and different areas damaged by the chemical lesions also contributed to the different behavioral readout.

The presence of tactile allodynia in persistent neuropathic pain may be associated with a shift of brain responses toward neural circuits that regulate the affective and motivational components of pain (33). Some clinical investigations show that working memory and attention impairments accompany chronic pain in patients (34, 35). These meaningful issues have indicated that there is a special area in the cerebral cortex involved in the modulation of pain, emotion, and cognition. It has been shown that activation of the ACC was involved in the chronic pain, accompanied by anxiety and/or depression (36). ACC neurons in layer V projected directly to the superficial laminae of the spinal dorsal horn, and stimulation of the ACC facilitated neuropathic pain responses (37, 38). The nucleus accumbens (NAc) contributed to an aversive learning signal that led to sustained pain intensity over time following peripheral nerve injury (21). The deactivation of the NAc played a causal role in the neuropathic pain phenotype (8). The mPFC-NAc connection is an accurate predictor of the transition

from subacute to chronic pain. It has also been reported that the PFC was involved in thalamic-PAG-dorsal horn top-down modulation of pain (39). The activation of PL excitatory neurons strongly activates the descending inhibitory pathway, which thus increases the pain threshold. Huang et al recently showed the existence and the anti-nociceptive function of the dmPFC-vlPAG pathway. Huang et al' study used various tracers and viruses to investigate the projections from mPFC to vlPAG (23). However, the synaptic evidence was not consolidation. In our study, the retro-transynaptic and antero-transynaptic viruses were adopted to confirm the certain projections from dmPFC to vlPAG for the first time.

Specific activation of pyramidal neurons in the PL, produced analgesic effects and improved anxiety-like behaviors following CFA injection (10). Meanwhile, specifically silencing parvalbumin (PV)-containing neurons in the dmPFC exerted obvious analgesic effects. Specifically activating these neurons worsened chronic pain-induced mechanical and heat hyperalgesia. Conditioned place preference scores and place escape/avoidance behavior have also been influenced by these PV-containing neurons in the PL (32). However, optogenetic either activation or deactivation of amygdala-PFC inputs did not affect anxiety behaviors in spared nerve injury (SNI) mice (23). Huang et al' study mainly focused on the analgesic effects of dmPFC-vlPAG neural pathway. While, we observed the effects of different neurons in the dmPFC, dmPFC-vlPAG neural pathway on the nociception-related affective behaviors. Our results indicated that specific activation of the dmPFC-vlPAG neural pathway, produced both analgesic and anxiolytic effects in CPNL chronic pain model.

In clinical practice, anodal transcranial current stimulation over the left dorsal lateral part of the PFC (dlPFC) ameliorated neuropathic pain. Analgesia might have occurred through modulation of the emotional pain network (40). In our study, chemogenetic activation of pyramidal neurons in the PFC also produced strong antinociceptive and anxiolytic effects. Our results suggested that the dmPFC was silenced under chronic pain conditions. Specific activation of the dmPFC-vlPAG neural pathway improved anxiety-like behaviors in the EPM, not in the OF, which indicated that the anxiolytic effects were not the result of analgesia. Specific activation of VGLUT2-containing

neurons or suppression of glutamate decarboxylases (GAD)-containing neurons in the vlPAG induced obvious analgesia and defensive behaviors in the mice (27, 28). These various behavioral outcomes suggest that the deactivation of the dmPFC-vlPAG neural pathway was involved in the initiation of anxiety-like behaviors assessed in the EPM.

The vlPAG is a significant modulator of both analgesic and fear behaviors in humans and rodents. Previous studies have showed that specific activation of VGLUT2-containing neurons in the vlPAG produced obvious analgesia and freezing behavior (28, 41). Tovote et al reported that this freezing behavior was produced by activation or disinhibition of vlPAG excitatory outputs to pre-motor targets in the magnocellular nucleus (Mc) of the medulla (28). However, it is still observed that VGLUT2+ neurons could also project to RVM directly involved in the descending pain inhibition. Therefore, it was speculated that analgesic and fear behaviors produced by activation of VGLUT2+ neurons in the vlPAG depend on vlPAG-RVM and vlPAG-Mc neuropathway, respectively. Rozeske et al reported that specific activation of the dmPFC-l/vlPAG pathway leads to low-fear states (reducing freezing levels) during contextual fear discrimination, which was similar to our results (42). A likely possibility is that excitatory dmPFC afferents impinge upon the GAD2+ neurons in the l/vlPAG (23), and thus inhibited vlPAG-Mc neuropathway. Besides, inhibition of GAD2+ neurons through CeA inhibitory inputs during cued fear expression would lead to fear responses, as already documented (28). Therefore, the activation of dmPFC excitatory inputs on the GAD2+ neurons in the l/vlPAG would induce the opposite effect, that is, a low-fear state. However, it is still observed that dmPFC excitatory inputs could also project onto VGLUT2+ neurons in the vlPAG directly involved in analgesic behaviors. Actually, the activation of the dmPFC-vlPAG neuropathway is not the cardinal pathway to modulate anxiety levels. Rozeske et al reported that the modulation of dmPFC-vlPAG in anxiety behaviors was specific to contextual discrimination paradigm (42). They performed optogenetic activation or inhibition of the dmPFC-l/vlPAG pathway in a classical auditory fear-conditioning and extinction paradigm associated with high- and low-freezing levels. Following conditioning, optogenetic activation of the dmPFC-l/vlPAG pathway did not reduce freezing levels. Huang et al recently showed that PFC-

vlPAG pathway was critical for the development of mechanical and thermal hypersensitivity after peripheral nerve injury (23). Specific activation of dmPFC-vlPAG produced both anti-nociception and anti-anxiety effects. Nevertheless, we think that the function of dmPFC-vlPAG on anxiolytic effects was not so comprehensive. In our study, activation of dmPFC-vlPAG only affected the anxiety behaviors in the EPM test and did not affected behaviors in the OF test. We hypothesized that the primary function of dmPFC on anxiety was finished through other targets, such as amygdala. The activation of the dmPFC-amygdala is the cardinal pathway to modulate anxiety levels. It was also demonstrated that manipulation of dmPFC has much more effects on anxiety behaviors than manipulation of dmPFC-vlPAG pathway in our investigation.

There were many findings regarding dmPFC deactivation in different pain models. Several possible molecular targets have been revealed. The pain and anxiety-like behaviors following CFA injection were related to the increased expression of cyclin-dependent kinase 5 (Cdk5). Knock-down of Cdk5 in the PL produced analgesic and anxiolytic effects (10). Bilateral intra-mPFC administration of the kappa-opioid receptors (KORs) antagonist nor-BNI increased central time in the OF, suggesting anxiolytic effects (43). Behaviorally, acute hyperpolarization-activated cyclic nucleotide-gated (HCN) channels blocked by local injection of ZD7288 in the dmPFC of SNI rats induced a decrease in cold allodynia (44). The loss of excitatory cholinergic modulation may also play a critical role in mPFC deactivation in neuropathic pain and underlie the mPFC-specific cognitive deficits that are comorbid with neuropathic pain (45). The impaired glutamatergic signaling contributed to the general deactivation of layer V PFC neurons following SNI surgery (17). Pain-associated dmPFC suppression has been thought to be driven by hyperactivity of the amygdala inputs to the dmPFC, which resulted in a group I metabotropic glutamate receptor-mediated increase in local GABAergic activity (19, 20). L-655, 708, a selective negative modulator at $GABA_A$ receptors reversed the alterations in hedonic behavior in the sucrose preference and social interaction tests (46). Recently, Huang et al' study showed that SNI leads to weakened endocannabinoid signaling in layer V of the mPFC, in turn causing a disinhibition of glutamatergic inputs into inhibitory neurons (23).

The present study was the first time to show the dmPFC-vlPAG neural pathway was involved in both pain modulation and anxiety-like behaviors. Activation of this neural pathway might be a straightforward and useful therapeutic strategy to both alleviate chronic pain and rescue anxiety/depression behaviors in chronic pain conditions.

Methods

Experimental animals

VGLUT2-ires-Cre mice were used to study the inputs of VGLUT2-ir neurons in the vlPAG by using rabies virus labeling system. Vgat-ires-Cre mice were used to study the effects of local inhibitory neurons in the dmPFC. For the other experiments, C57BL/6J mice were used. All mice (male, 8-10 weeks of age, 20-25 g) were housed under a 12 h light/dark cycle with lights on at 7 am and food and water provided *ad libitum*, which were all purchased from Jackson Laboratories. Mice were housed in clear plastic cages in a controlled environment at a constant temperature of 23 ℃ and humidity of 50 ± 10%.

CPNL model

The CPNL model was established to observe pain- and anxiety-related behaviors following previous procedures (37, 47). Briefly, mice were anesthetized by an intraperitoneal (*i.p.*) injection of 2% sodium pentobarbital (40 mg/kg). The CPN was visible between the anterior and posterior groups of muscles, running almost transversely. The left CPN was slowly ligated with chromic gut suture 5–0 until contraction of the dorsiflexor of the foot was visible as twitching of the digits. The skin was then sutured and cleaned. Sham surgery was conducted in the same manner, but the nerve was not ligated. The mice were used for behavioral studies on postsurgical days 1, 3, 7, and 14.

Measurement of sensitivity to mechanical stimuli

The measurements were based on our previous publications (48, 49). Mice were habituated to the testing environment for 3 days before baseline testing and were then placed under inverted plastic boxes (7*7*10 cm) on an elevated mesh floor and allowed

to habituate for 30 min before the threshold testing. A logarithmic series of 8 calibrated Semmes-Weinstein monofilaments (*von* Frey hairs; Stoelting, Kiel, WI, USA) was applied to the plantar surface of the paw that received nerve ligation and contralateral paw. Positive responses included licking, biting, and sudden withdrawing of the hindpaws. Log stiffness of the hairs was determined by log10 (milligrams x 10). A *von* Frey filament was applied 5 times (3 seconds for each stimulus) to each testing area. The minimum bending force of the *von* Frey filament able to evoke 3 occurrences of the paw withdrawal reflex was expressed as a 50% withdrawal threshold. The stimulus was stopped if the threshold exceeded 10.0 g (cutoff value). Mechanical allodynia was assessed based on the responsiveness of the hindpaws to the application of a particular *von* Frey filament (0.04 g). Ten trails were carried out each time, and the results were expressed as a percentage of positive responses. All tests were performed in a blind manner.

Open field and elevated plus maze tests

The open field (OF) test was conducted according to our previous studies (50, 51). Mice were placed at the center of a cubic chamber that measured 50 cm (W) × 50 cm (L) × 45 cm (H). The locomotor activity of mice for 15 min was monitored by an automated analyzing system. The total distance traveled was used as a measure of the locomotion, and the percentage of time spent in the central area (% of total time) was used to evaluate anxiety-like behavior by off-line analysis. All animals were habituated to the testing room for 30 min before the OF test. The behavioral room was dimly illuminated with indirect white lighting.

The elevated plus maze (EPM) test was conducted according to our previous studies (52, 53). The EPM is made of a white Plexiglas apparatus consisting of two opposing open arms (OA, 30 × 5 cm), two opposing closed arms (CA, 30 × 5 × 25 cm), and a central area measuring 5 × 5 cm. The plus-shaped platform was 50 cm above the floor. Generally, mice were placed individually into the center area of the maze facing one of the OAs and were allowed to explore for 5 min. The number of OA and CA entries and time spent in the OAs and CAs were recorded by an automated analysis system. Only when all 4 paws crossed out of the central zone was the animal considered in an OA or a CA. The percentage of time spent in the OAs (% of total time) and the percentage of

entries into the OAs (% of total entries) were measured to evaluate general anxiety levels. The environmental conditions and the habituation protocol for the EPM test were the same as those of the OF test.

Stereotaxic kainic acid, tracer and virus injection

The injection procedures have been described in our previous studies (54, 55). In brief, mice were anesthetized with 2% sodium pentobarbital (40 mg/kg, *i.p.*). A midline opening was made in the skull with a dental drill to insert a glass micropipette connected to a microsyringe (1 μl, Hamilton, Reno, NV, USA) into the target site. The detailed injection information is presented in **Table S1**. The mice with the virus infection were allowed to recover for 4 weeks prior to the behavioral experiments (56).

For cell-type-specific retrograde transsynaptic tracing, Cre-dependent AAV2/9-DIO-EGFP-TVA and AAV2/9-DIO-RG were mixed with an equal volume prior to viral injections. Then, 300 nl of the AAV mixture was stereotaxically injected into the vlPAG of VGLUT2-ires-Cre mice, which allowed EGFP-TVA and RG selective expression in VGLUT2-containing neurons. After 4 weeks of recovery and AAV expression, 300 nl RV-EnvA-ΔG-dsRed was injected into the same location in a biosafety level-2 environment. After 1 week of rabies virus infection and transsynaptic spread (57, 58), the animals were sacrificed.

Fiber optic ferrules or cannula implantation

For optogenetic experiments, a custom-made ferrule with fiber optic (100 μm in core diameter, Doric Lenses) was subsequently placed above the vlPAG and fixed on the skull with bone screws, super glue and dental cement (Parkell; Metabond). Unless otherwise indicated, the control animals used in this study were animals with the same genetic background injected with AAV2/2-CaMKIIα-EYFP, which also received fiber optic implantation in the vlPAG.

For microinjection of drugs into the dmPFC, a 3.0 mm length guide cannula (6202, OD 0.56 x ID 0.38 mm, RWD, Shenzhen, China) was stereotaxically implanted, aimed at the contralateral dmPFC, fixed to the skull with bone screws, super glue, dental cement, and a dummy cannula was inserted into the guide cannula. After guide cannula

implantation and a 1-week recovery, mice were tested for pain-related and anxiety-like behaviors.

Behavioral tests with optogenetic, chemogenetic, and pharmacological approaches

Optogenetic experiments were performed similar to previous studies with modification (10, 59). Mice with fiber optic ferrules in the vlPAG were photostimulated by attaching the ferrule to a fiber optic cable with a rotary joint (Doric lenses), followed by another fiber optic cable that was then attached to a fiber-coupled 473 nm blue laser (BOGS-1, Beijing Bio-Gold Biotech Co. Ltd). Laser power output from the fiber optic cable was measured using a photometer (Thor Labs) and set to ~12 mW / mm^2 as power loss through the ferrule-cable connection was 10-20%. For the *von* Frey test, a 2 min stimulation (473 nM at 20 Hz, 10 ms pulse) with a 2 min break following each stimulation was performed for each animal, until the mechanical thresholds were detected. For the OF and EPM tests, the behavior over a total of 9 min was recorded, which included 3-min of photostimulation, 3-min break, and 3-min photostimulation with the same blue light frequency and power intensity.

For the chemogenetic test, the mice following virus injection received CNO 1 mg/kg (Sigma, St. Louis, MO, USA) or saline 50 μl *i.p.* injection, followed by detection of the pain thresholds and the recording of behaviors in the OF and EPM.

0.4 μl saline or 0.1 μg of bicuculline (Sigma) or 0.4 nmol of LY367385 (Tocris Bioscience, Bristol, United Kingdom) were injected at a rate of 50 nl/min using a 3.2 mm length injection cannula connected to a Pump Elite 11 infusion pump (Harvard Apparatus) via a polyethylene tube. Mice were tested in the behavioral assessments by observers blinded to the animal groups. Similarly, the mechanical thresholds of the bilateral hindpaws and behaviors in the OF and EPM were detected or recorded.

Immunohistochemical and immunofluorescence histochemical staining

The procedures were performed as previously described (48, 55). After deep anesthesia using pentobarbital (100 mg/kg, *i.p.*), and perfusion with 0.1 M phosphate buffer (PB, pH 7.4) containing 4% paraformaldehyde, the whole brain was removed and postfixed for 4 h and then immersed in 30% sucrose in 0.1 M PB for 48 h at 4 ℃. Transverse

forebrain containing the dmPFC, vlPAG, or RVM sections were cut at 40 μm thickness on a cryostat (Leica CM1800, Heidelberg, Germany) at -20 ℃, and sections were collected serially into dishes containing 0.01 M phosphate-buffered saline (PBS, pH 7.4).

Immunohistochemical staining for fluoro-gold (FG) or biotinylated dextran amine (BDA) was performed with an avidin-biotin-peroxidase complex (ABC) method. The sections were blocked for 0.5 h at room temperature (RT, 20-25 ℃). The sections were incubated overnight at RT with guinea pig (Gp) anti-FG antiserum (1:200; NM-101, PROTOS BIOTECH CORP, New York, NY, USA), followed by incubation with donkey anti-Gp IgG (1:500; AP193B, Millipore, Billerica, MA, USA) for 5 h. Finally, sections (or sections used for detecting BDA) were incubated with the ABC-Elite kit (1:100; A-2001, Vector Laboratories, Burlingame, CA, USA) at RT for 2 h, and then sections were further incubated in a solution containing 0.05 M Tris-HCl, 0.13% diaminobenzidine, and 0.005% hydrogen peroxide for 20 to 30 min to complete the diaminobenzidine reaction. Finally, all sections were mounted onto gelatin-coated glass slides, air dried, dehydrated in a graded series of diluted ethanol, cleared in xylene, and cover slipped.

The procedures for immunofluorescent histochemical staining were the same as those previously described (55, 60, 61). The dmPFC sections of the mice that received the FG or virus injection, or the mice that received a cannula implantation were used to evaluate the double staining of FG/CaMKII, GAD67/FG, NeuN/FG, NeuN/GFAP or Fos/DAPI, Biocytin/DAPI or the triple staining of mCitrin/GAD67/Fos, EYFP/FG/Synapsin, 5-HT/FG/VGLUT2. The vlPAG sections of the mice that received the dmPFC AAV2/2-CaMKIIα-EYFP injection and the RVM FG injection or mice that received the dmPFC AAV2/2-CaMKIIα-hChR2-EYFP injection were used to evaluate the single staining of FG or Fos, EYFP/FG respectively (**Table S2**). Finally, all of the sections were then mounted onto glass slides and observed with laser scanning confocal microscopy (FV1000, Olympus, Japan) under appropriate filters.

in situ hybridization histochemistry combined with retrograde tract tracing

Fluorescent *in situ* hybridization (FISH) was performed as previously described (62, 63). After a survival period of 1 week, the mice injected with FG into the vlPAG or RVM were perfused, and the brains were cut into 20-μm thick transverse sections. Then, the sections were hybridized with digoxigenin-labeled VGLUT1 or VGLUT2 riboprobe. After washes and ribonuclease A treatment, the hybridized sections were incubated overnight at RT with a mixture of 1:2,000-diluted peroxidase-conjugated anti-digoxigenin sheep antibody (11-207-733-910, Roche Diagnostics, Basel, Switzerland) and 1:200-diluted Gp anti-FG antibody. To amplify the signals for VGLUT1 or VGLUT2 mRNA, we performed the biotinylated tyramine (BT)-glucose oxidase (GO) amplification method (64). Subsequently, the sections were incubated with 10 μg/ml Alexa488-conjugated streptavidin (S-11223, Invitrogen) for 2 h and then with 10 μg/ml Alexa594-conjugated goat antibody to Gp IgG (Invitrogen) for 4 h. Finally, all of the sections were mounted onto glass slides and observed with laser scanning confocal microscopy.

Electrophysiology

Coronal brain slices containing dmPFC were prepared following our previous studies (60, 65). Transverse slices (300 μm thick) were cut on a vibrating microtome (Leica VT 1200s, Heidelberger, Nussloch, Germany) in 4℃. The slices were transferred to a submerged chamber containing artificial cerebrospinal fluid containing the following reagents: 124 mM NaCl, 2.5 mM KCl, 2 mM $CaCl_2$, 2 mM $MgSO_4$, 25 mM $NaHCO_3$, 1 mM NaH_2PO_4, 10 mM glucose, 1 mM ascorbate, and 3 mM sodium pyruvate. The recordings were made in voltage-clamp or current-clamp mode by using Axon 700B amplifier (Axon Instruments, Foster City, CA, USA). Pclamp software (v. 10.02, Axon Instruments) was used to acquire and analyze the data. The recording pipettes (3–6 MΩ) filled with a solution containing: 130 mM potassium-gluconate, 5 mM NaCl, 15 mM KCl, 0.4 mM ethylene glycol tetraacetic acid (EGTA), 10 mM 4-(2-hydroxyethyl)-1-piperazineethanesulfonic acid (HEPES), 4 mM Mg-ATP, and 0.3 mM Na_2-GTP (adjusted to pH 7.3 with KOH) were used for recording. For sEPSC recording, cells were voltage clamped at -70 mV. The recordings were performed on retroBeads-containing pyramidal neurons, eGFP-expressing pyramidal neurons, or mCherry-

expressing inhibitory neurons in the dmPFC that were visualized under epifluorescence using a filter set (U-HGLGPS, Olympus) with a monochrome CCD camera (IR-1000E, DAGE-MTI, Michigan, USA) and monitor. In cases of retroBeads tracing, 0.2% biocytin (Sigma-Aldrich, St. Louis, MO, USA) was introduced into the recording solution to identify the recorded neurons. The action potentials were detected in response to supra-threshold current injections in the current clamp mode. Depolarizing currents of 0-300 pA (400 ms duration) were delivered in increments of 20 pA. Optical stimulation (473 nm) was applied with a custom laser fiber. The stimulation pattern was similar to that used in vivo (5 Hz, 10 Hz, and 20 Hz pulse trains). Blue light was applied through a 40 objective over the field of view of the patched cell. Picrotoxin (100 μM) was used to block inhibitory synaptic transmission from the inhibitory neurons to the dmPFC-vlPAG projection neurons. CNO evoked currents were recorded in voltage-clamp mode with membrane potential held at 70 mV, and cells were stimulated using 40μM CNO.

Western blot analysis

Mice were sacrificed after inducing deep anesthesia using pentobarbital (100 mg/kg, *i.p.*), and then the whole brain was quickly removed. The dmPFC was collected and homogenized with a hand-held pestle in sodium dodecyl sulfate (SDS) sample buffer. The electrophoresis samples were heated at 100 ℃ for 5 min and loaded onto 10% SDS-polyacrylamide gels with standard Laemmli solutions (Bio-Rad Laboratories, CA, USA). The proteins were electroblotted onto a polyvinylidene difluoride membrane (PVDF, Immobilon-P, Millipore). The membranes were placed in a blocking solution for 1 h and incubated overnight under gentle agitation with primary antibody rabbit anti-$GABA_AR$ (1:1000; ab72446, Abcam) or rabbit anti-mGluR1 (1:1000; ab82211, Abcam) and mouse anti-β-actin (1:5000; Sigma). Bound primary antibodies were detected with a horseradish peroxidase (HRP)-conjugated anti-rabbit (1:5000; ZB-2301, ZSGB-BIO, Beijing, China) or anti-mouse secondary antibody (1:5000; ZB-2305, ZSGB-BIO). All reactions were detected by the enhanced chemiluminescence (ECL) detection method. The densities of protein blots were analyzed using Labworks

Software (Ultra-Violet Products, UK). The densities of $GABA_AR$, mGluR1 and β-actin immunoreactive bands were quantified with background subtraction.

Statistics

Values were reported as the mean ± standard error of the mean (SEM). The behavioral data were analyzed by one-way or two-way repeated measures ANOVA, with Bonferroni post hoc tests or Turkey's post hoc test, paired *t* test, Student't *t* test. Student's *t* test were used for immunofluorescence analysis or analyzing western blot data. The comparison of electrophysiology data used Two-way repeated measures ANOVA with Bonferroni post hoc test, Student't *t* test. Statistical methods in detailed were indicated when used. Statistical analyses were performed using Prism 6 (v6.0e, GraphPad, San Diego, CA). Normality and equal variance tests were performed for all statistical analyses. $P < 0.05$ was considered statistically significant.

Study approval

All experimental procedures received prior approval from the Animal Use and Care Committee for Research and Education of The Fourth Military Medical University (Xi'an, China), and followed ethical guidelines for the investigation of experimental pain in conscious animals.

Author contributions

Y.Q. L., Y.L. D., X. L., and J.B. Y. conceived the project and designed the experiments; J.B. Y., F. L., Z.Y. W., J. H., R. R., Y.N. P., and H. L. performed immunofluorescence staining; Y.C. L, J.B. Y., T. Z., H.X. L., J. Y., and T. D. finished the dmPFC lesion and behavior tests; S.H. L., Y. S., Y. S., and T. C. carried out the optogenetic and chemogenetic investigations; S.H. L., Y. S., and Y. B. performed the pharmacological tests; Y.Q. L., Y.L. D., X. L., Z.F. C., and J.B. Y. wrote the manuscript. W.J. Z., J. C., Y.C. L., and W.D. Z. finished the supplementary experiments. All authors approved the manuscript.

Acknowledgments

This work was supported by National Natural Science Foundation of China (grant number 81620108008 to YQ Li; 31871061 and 31671087 to YL Dong; 81801099 to JB Yin), Hainan ZDYF2018153 to YQ Li, China Postdoctoral Science Foundation Special Funded Project (2019TQ0135) and intramural grant of the Fourth Military Medical University (2015D06 to JB Yin). JB Yin was also supported by the China Scholar Council.

Reference

1. Malfliet A, Coppieters I, Van Wilgen P, Kregel J, De Pauw R, Dolphens M, and Ickmans K. Brain changes associated with cognitive and emotional factors in chronic pain: A systematic review. *European journal of pain.* 2017;21(5):769-86.
2. Simons LE, Elman I, and Borsook D. Psychological processing in chronic pain: a neural systems approach. *Neurosci Biobehav Rev.* 2014;39(61-78.
3. Block CK, and Brock J. The relationship of pain catastrophizing to heightened feelings of distress. *Pain Manag Nurs.* 2008;9(2):73-80.
4. Price DD. Psychological and neural mechanisms of the affective dimension of pain. *Science.* 2000;288(5472):1769-72.
5. Gambassi G. Pain and depression: the egg and the chicken story revisited. *Arch Gerontol Geriatr.* 2009;49 Suppl 1(103-12.
6. Jann MW, and Slade JH. Antidepressant agents for the treatment of chronic pain and depression. *Pharmacotherapy.* 2007;27(11):1571-87.
7. Jurik A, Auffenberg E, Klein S, Deussing JM, Schmid RM, Wotjak CT, and Thoeringer CK. Roles of prefrontal cortex and paraventricular thalamus in affective and mechanical components of visceral nociception. *Pain.* 2015;156(12):2479-91.
8. Lee M, Manders TR, Eberle SE, Su C, D'Amour J, Yang R, Lin HY, Deisseroth K, Froemke RC, and Wang J. Activation of corticostriatal circuitry relieves chronic neuropathic pain. *J Neurosci.* 2015;35(13):5247-59.
9. Martinez E, Lin HH, Zhou H, Dale J, Liu K, and Wang J. Corticostriatal Regulation of Acute Pain. *Front Cell Neurosci.* 2017;11(146.
10. Wang GQ, Cen C, Li C, Cao S, Wang N, Zhou Z, Liu XM, Xu Y, Tian NX, Zhang Y, et al. Deactivation of excitatory neurons in the prelimbic cortex via Cdk5 promotes pain sensation and anxiety. *Nat Commun.* 2015;6(7660.
11. Barbas H. Anatomic basis of cognitive-emotional interactions in the primate prefrontal cortex. *Neurosci Biobehav Rev.* 1995;19(3):499-510.
12. Lee D, Rushworth MF, Walton ME, Watanabe M, and Sakagami M. Functional specialization of the primate frontal cortex during decision making. *J Neurosci.* 2007;27(31):8170-3.
13. Rushworth MF, Noonan MP, Boorman ED, Walton ME, and Behrens TE. Frontal cortex and reward-guided learning and decision-making. *Neuron.* 2011;70(6):1054-69.

14. Friedman A, Homma D, Gibb LG, Amemori K, Rubin SJ, Hood AS, Riad MH, and Graybiel AM. A Corticostriatal Path Targeting Striosomes Controls Decision-Making under Conflict. *Cell.* 2015;161(6):1320-33.
15. Salzman CD, and Fusi S. Emotion, cognition, and mental state representation in amygdala and prefrontal cortex. *Annu Rev Neurosci.* 2010;33(173-202.
16. Sun H, and Neugebauer V. mGluR1, but not mGluR5, activates feed-forward inhibition in the medial prefrontal cortex to impair decision making. *J Neurophysiol.* 2011;106(2):960-73.
17. Kelly CJ, Huang M, Meltzer H, and Martina M. Reduced Glutamatergic Currents and Dendritic Branching of Layer 5 Pyramidal Cells Contribute to Medial Prefrontal Cortex Deactivation in a Rat Model of Neuropathic Pain. *Front Cell Neurosci.* 2016;10(133.
18. Metz AE, Yau HJ, Centeno MV, Apkarian AV, and Martina M. Morphological and functional reorganization of rat medial prefrontal cortex in neuropathic pain. *Proc Natl Acad Sci U S A.* 2009;106(7):2423-8.
19. Ji G, and Neugebauer V. Pain-related deactivation of medial prefrontal cortical neurons involves mGluR1 and GABA(A) receptors. *J Neurophysiol.* 2011;106(5):2642-52.
20. Ji G, Sun H, Fu Y, Li Z, Pais-Vieira M, Galhardo V, and Neugebauer V. Cognitive impairment in pain through amygdala-driven prefrontal cortical deactivation. *J Neurosci.* 2010;30(15):5451-64.
21. Baliki MN, Petre B, Torbey S, Herrmann KM, Huang L, Schnitzer TJ, Fields HL, and Apkarian AV. Corticostriatal functional connectivity predicts transition to chronic back pain. *Nat Neurosci.* 2012;15(8):1117-9.
22. Mansour AR, Baliki MN, Huang L, Torbey S, Herrmann KM, Schnitzer TJ, and Apkarian AV. Brain white matter structural properties predict transition to chronic pain. *Pain.* 2013;154(10):2160-8.
23. Huang J, Gadotti VM, Chen L, Souza IA, Huang S, Wang D, Ramakrishnan C, Deisseroth K, Zhang Z, and Zamponi GW. A neuronal circuit for activating descending modulation of neuropathic pain. *Nat Neurosci.* 2019;22(10):1659-68.
24. Francois A, Low SA, Sypek EI, Christensen AJ, Sotoudeh C, Beier KT, Ramakrishnan C, Ritola KD, Sharif-Naeini R, Deisseroth K, et al. A Brainstem-Spinal Cord Inhibitory Circuit for Mechanical Pain Modulation by GABA and Enkephalins. *Neuron.* 2017;93(4):822-39 e6.
25. Millan MJ. Descending control of pain. *Prog Neurobiol.* 2002;66(6):355-474.
26. Wu SX, Wang W, Li H, Wang YY, Feng YP, and Li YQ. The synaptic connectivity that underlies the noxious transmission and modulation within the superficial dorsal horn of the spinal cord. *Prog Neurobiol.* 2010;91(1):38-54.
27. Samineni VK, Grajales-Reyes JG, Copits BA, O'Brien DE, Trigg SL, Gomez AM, Bruchas MR, and Gereau RWt. Divergent Modulation of Nociception by Glutamatergic and GABAergic Neuronal Subpopulations in the Periaqueductal Gray. *eNeuro.* 2017;4(2).
28. Tovote P, Esposito MS, Botta P, Chaudun F, Fadok JP, Markovic M, Wolff SB, Ramakrishnan C, Fenno L, Deisseroth K, et al. Midbrain circuits for defensive behaviour. *Nature.* 2016;534(7606):206-12.
29. Zingg B, Chou XL, Zhang ZG, Mesik L, Liang F, Tao HW, and Zhang LI. AAV-Mediated Anterograde Transsynaptic Tagging: Mapping Corticocollicular Input-Defined Neural Pathways for Defense Behaviors. *Neuron.* 2017;93(1):33-47.
30. Zingg B, Peng B, Huang J, Tao HW, and Zhang LI. Synaptic Specificity and Application of

Anterograde Transsynaptic AAV for Probing Neural Circuitry. *J Neurosci.* 2020;40(16):3250-67.

31. Kvitsiani D, Ranade S, Hangya B, Taniguchi H, Huang JZ, and Kepecs A. Distinct behavioural and network correlates of two interneuron types in prefrontal cortex. *Nature.* 2013;498(7454):363-6.

32. Zhang Z, Gadotti VM, Chen L, Souza IA, Stemkowski PL, and Zamponi GW. Role of Prelimbic GABAergic Circuits in Sensory and Emotional Aspects of Neuropathic Pain. *Cell Rep.* 2015;12(5):752-9.

33. Chang PC, Centeno MV, Procissi D, Baria A, and Apkarian AV. Brain activity for tactile allodynia: a longitudinal awake rat functional magnetic resonance imaging study tracking emergence of neuropathic pain. *Pain.* 2017;158(3):488-97.

34. Baker KS, Gibson S, Georgiou-Karistianis N, Roth RM, and Giummarra MJ. Everyday Executive Functioning in Chronic Pain: Specific Deficits in Working Memory and Emotion Control, Predicted by Mood, Medications, and Pain Interference. *The Clinical journal of pain.* 2016;32(8):673-80.

35. Moriarty O, McGuire BE, and Finn DP. The effect of pain on cognitive function: a review of clinical and preclinical research. *Prog Neurobiol.* 2011;93(3):385-404.

36. Zhuo M. Neural Mechanisms Underlying Anxiety-Chronic Pain Interactions. *Trends Neurosci.* 2016;39(3):136-45.

37. Chen T, Koga K, Descalzi G, Qiu S, Wang J, Zhang LS, Zhang ZJ, He XB, Qin X, Xu FQ, et al. Postsynaptic potentiation of corticospinal projecting neurons in the anterior cingulate cortex after nerve injury. *Molecular pain.* 2014;10(33.

38. Chen T, Wang W, Dong YL, Zhang MM, Wang J, Koga K, Liao YH, Li JL, Budisantoso T, Shigemoto R, et al. Postsynaptic insertion of AMPA receptor onto cortical pyramidal neurons in the anterior cingulate cortex after peripheral nerve injury. *Mol Brain.* 2014;7(76.

39. Bingel U, Tracey I, and Wiech K. Neuroimaging as a tool to investigate how cognitive factors influence analgesic drug outcomes. *Neurosci Lett.* 2012;520(2):149-55.

40. Ayache SS, Palm U, Chalah MA, Al-Ani T, Brignol A, Abdellaoui M, Dimitri D, Sorel M, Creange A, and Lefaucheur JP. Prefrontal tDCS Decreases Pain in Patients with Multiple Sclerosis. *Front Neurosci.* 2016;10(147.

41. Taylor NE, Pei J, Zhang J, Vlasov KY, Davis T, Taylor E, Weng FJ, Van Dort CJ, Solt K, and Brown EN. The Role of Glutamatergic and Dopaminergic Neurons in the Periaqueductal Gray/Dorsal Raphe: Separating Analgesia and Anxiety. *eNeuro.* 2019;6(1).

42. Rozeske RR, Jercog D, Karalis N, Chaudun F, Khoder S, Girard D, Winke N, and Herry C. Prefrontal-Periaqueductal Gray-Projecting Neurons Mediate Context Fear Discrimination. *Neuron.* 2018;97(4):898-910 e6.

43. Tejeda HA, Hanks AN, Scott L, Mejias-Aponte C, Hughes ZA, and O'Donnell P. Prefrontal Cortical Kappa Opioid Receptors Attenuate Responses to Amygdala Inputs. *Neuropsychopharmacology.* 2015;40(13):2856-64.

44. Cordeiro Matos S, Zhang Z, and Seguela P. Peripheral Neuropathy Induces HCN Channel Dysfunction in Pyramidal Neurons of the Medial Prefrontal Cortex. *J Neurosci.* 2015;35(38):13244-56.

45. Radzicki D, Pollema-Mays SL, Sanz-Clemente A, and Martina M. Loss of M1 Receptor Dependent Cholinergic Excitation Contributes to mPFC Deactivation in Neuropathic Pain. *J Neurosci.* 2017;37(9):2292-304.

46. Fischell J, Van Dyke AM, Kvarta MD, LeGates TA, and Thompson SM. Rapid Antidepressant Action and Restoration of Excitatory Synaptic Strength After Chronic Stress by Negative Modulators of Alpha5-Containing GABAA Receptors. *Neuropsychopharmacology.* 2015;40(11):2499-509.
47. Vadakkan KI, Jia YH, and Zhuo M. A behavioral model of neuropathic pain induced by ligation of the common peroneal nerve in mice. *J Pain.* 2005;6(11):747-56.
48. Yin JB, Zhou KC, Wu HH, Hu W, Ding T, Zhang T, Wang LY, Kou JP, Kaye AD, and Wang W. Analgesic Effects of Danggui-Shaoyao-San on Various "Phenotypes" of Nociception and Inflammation in a Formalin Pain Model. *Mol Neurobiol.* 2016;53(10):6835-48.
49. Zhao YQ, Wang HY, Yin JB, Sun Y, Wang Y, Liang JC, Guo XJ, Tang K, and Wang YT. The Analgesic Effects of Celecoxib on the Formalin-induced Short- and Long-term Inflammatory Pain. *Pain Physician.* 2017;20(4):E575-E84.
50. Wu HH, Yin JB, Zhang T, Cui YY, Dong YL, Chen GZ, and Wang W. Inhibiting spinal neuron-astrocytic activation correlates with synergistic analgesia of dexmedetomidine and ropivacaine. *PloS one.* 2014;9(3):e92374.
51. Zhai MZ, Wu HH, Yin JB, Cui YY, Mei XP, Zhang H, Zhu X, Shen XF, Kaye AD, and Chen GZ. Dexmedetomidine Dose-Dependently Attenuates Ropivacaine-Induced Seizures and Negative Emotions Via Inhibiting Phosphorylation of Amygdala Extracellular Signal-Regulated Kinase in Mice. *Mol Neurobiol.* 2016;53(4):2636-46.
52. Xia L, Zhai M, Wang L, Miao D, Zhu X, and Wang W. FGF2 blocks PTSD symptoms via an astrocyte-based mechanism. *Behavioural brain research.* 2013;256(472-80.
53. Zhang MM, Liu SB, Chen T, Koga K, Zhang T, Li YQ, and Zhuo M. Effects of NB001 and gabapentin on irritable bowel syndrome-induced behavioral anxiety and spontaneous pain. *Mol Brain.* 2014;7(47.
54. Chen T, Wang XL, Qu J, Wang W, Zhang T, Yanagawa Y, Wu SX, and Li YQ. Neurokinin-1 receptor-expressing neurons that contain serotonin and gamma-aminobutyric acid in the rat rostroventromedial medulla are involved in pain processing. *J Pain.* 2013;14(8):778-92.
55. Yin JB, Wu HH, Dong YL, Zhang T, Wang J, Zhang Y, Wei YY, Lu YC, Wu SX, Wang W, et al. Neurochemical properties of BDNF-containing neurons projecting to rostral ventromedial medulla in the ventrolateral periaqueductal gray. *Front Neural Circuits.* 2014;8(137.
56. Paxinos G WC ed. *The rat brain in stereotaxic coordinates, Ed 5.* Amsterdam: Elsevier; 2005.
57. Wall NR, Wickersham IR, Cetin A, De La Parra M, and Callaway EM. Monosynaptic circuit tracing in vivo through Cre-dependent targeting and complementation of modified rabies virus. *Proc Natl Acad Sci U S A.* 2010;107(50):21848-53.
58. Watabe-Uchida M, Zhu L, Ogawa SK, Vamanrao A, and Uchida N. Whole-brain mapping of direct inputs to midbrain dopamine neurons. *Neuron.* 2012;74(5):858-73.
59. Yu YQ, Barry DM, Hao Y, Liu XT, and Chen ZF. Molecular and neural basis of contagious itch behavior in mice. *Science.* 2017;355(6329):1072-6.
60. Chen T, Li J, Feng B, Hui R, Dong YL, Huo FQ, Zhang T, Yin JB, Du JQ, and Li YQ. Mechanism Underlying the Analgesic Effect Exerted by Endomorphin-1 in the rat Ventrolateral Periaqueductal Gray. *Mol Neurobiol.* 2016;53(3):2036-53.
61. Liang SH, Yin JB, Sun Y, Bai Y, Zhou KX, Zhao WJ, Wang W, Dong YL, and Li YQ. Collateral projections from the lateral parabrachial nucleus to the paraventricular thalamic nucleus and the central amygdaloid nucleus in the rat. *Neurosci Lett.* 2016;629(245-50.

62. Ge SN, Li ZH, Tang J, Ma Y, Hioki H, Zhang T, Lu YC, Zhang FX, Mizuno N, Kaneko T, et al. Differential expression of VGLUT1 or VGLUT2 in the trigeminothalamic or trigeminocerebellar projection neurons in the rat. *Brain structure & function.* 2014;219(1):211-29.
63. Liu X, Zhang C, Wang D, Zhang H, Liu X, Li J, and Wang M. Proprioceptive mechanisms in occlusion-stimulated masseter hypercontraction. *Eur J Oral Sci.* 2017;125(2):127-34.
64. Kuramoto E, Furuta T, Nakamura KC, Unzai T, Hioki H, and Kaneko T. Two types of thalamocortical projections from the motor thalamic nuclei of the rat: a single neuron-tracing study using viral vectors. *Cereb Cortex.* 2009;19(9):2065-77.
65. Chen T, Taniguchi W, Chen QY, Tozaki-Saitoh H, Song Q, Liu RH, Koga K, Matsuda T, Kaito-Sugimura Y, Wang J, et al. Top-down descending facilitation of spinal sensory excitatory transmission from the anterior cingulate cortex. *Nat Commun.* 2018;9(1):1886.

Figure Legends

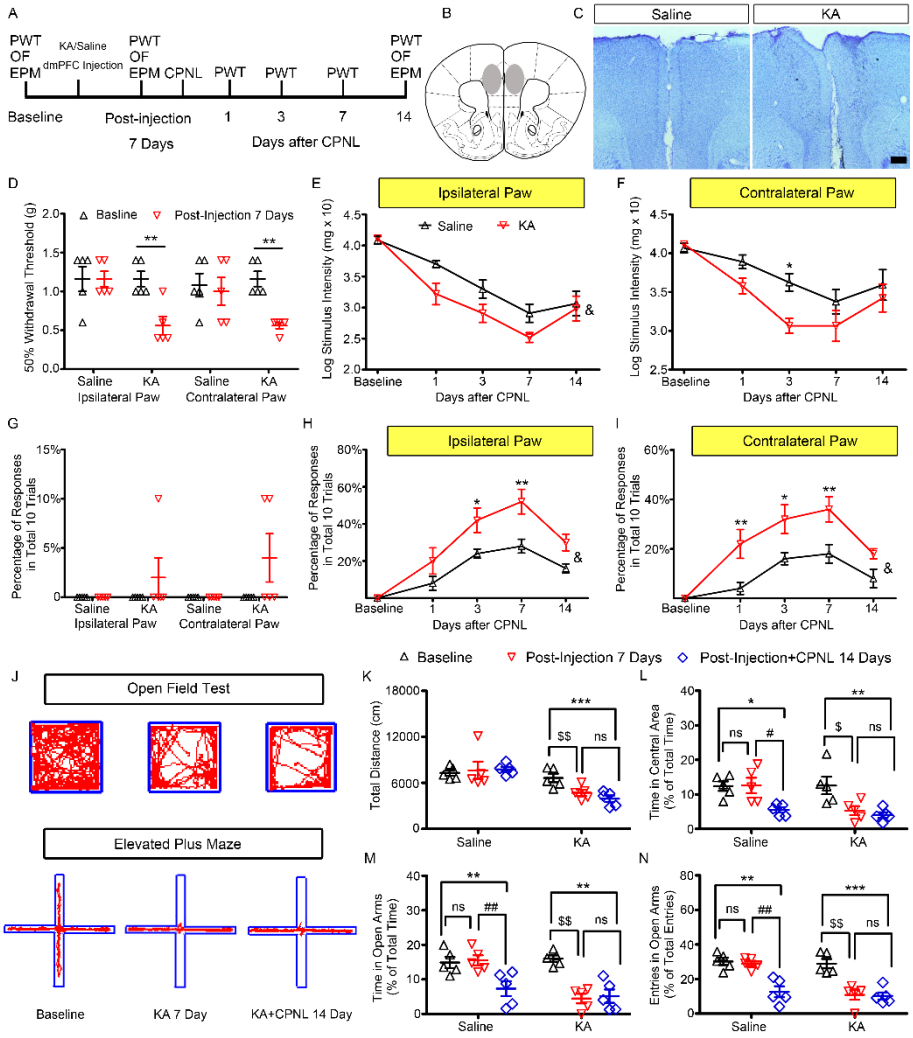

Figure 1. Bilateral lesions of the dmPFC worsen CPNL-induced mechanical nociception and anxiety-like behaviors.

(**A-B**) Representative schematic diagrams of the KA injection into the dmPFC and procedures for the behavioral tests. (**C**) Nissl staining of the dmPFC after KA or saline dmPFC injections. Scale bar=200 μm. (**D**) Mechanical thresholds at baseline and 7 days after saline or KA dmPFC injections (***P*<0.01, paired *t* test, n=5). Mechanical thresholds of the ipsilateral (**E**) and contralateral (**F**) hindpaws following CPNL with saline or KA dmPFC injections (E: $F_{(1,32)}$=6.07, *P*=0.04; $^{\&}P$<0.05; F: $F_{(1,32)}$=4.22, *P*=0.07; two-way repeated measures ANOVA, with Bonferroni post hoc tests, **P*<0.05, n=5). (**G**) Responses to non-nociceptive stimulation at baseline and 7 days after saline or KA dmPFC injections (n=5). Responses to non-nociceptive stimulation of the ipsilateral (**H**) and contralateral (**I**) hindpaws following CPNL with saline or KA

dmPFC injections (H: $F_{(1,32)}$=9.80, P=0.014; $^{\&}P$<0.05; I: $F_{(1,32)}$=10.68, P=0.011; $^{\&}P$<0.05, two-way repeated measures ANOVA, with Bonferroni post hoc tests, *P<0.05, **P<0.01, n=5). (**J**) Schematic traces of the OF and EPM test at baseline, 7 days after KA injection, and 7 days after KA injection + 14 days after CPNL. The total distance traveled (**K**) and the percentage of time in the central area (**L**) in the OF (Saline injection, K: $F_{(2, 8)}$=0.11, P=0.90; L: $F_{(2, 8)}$=5.97, P=0.03; KA injection, K: $F_{(2, 8)}$=24.97, P<0.001; L: $F_{(2, 8)}$=9.33, P<0.01; one-way repeated measures ANOVA with Turkey's post hoc test, *P<0.05, **P<0.01, ***P<0.001, $^{\$}P$<0.05, $^{\$\$}P$<0.01, $^{\#}P$<0.05, n=5). The percentage of time in (**M**) and percentage of entries into (**N**) the open arms in the EPM (Saline injection, M: $F_{(2, 8)}$=13.22, P<0.01; N: $F_{(2, 8)}$=20.28, P<0.001; KA injection, M: $F_{(2, 8)}$=17.34, P<0.01; N: $F_{(2, 8)}$=23.23, P<0.001; one-way repeated measures ANOVA with Turkey's post hoc test, **P<0.01, ***P<0.001, $^{\$\$}P$<0.01, $^{\#\#}P$<0.01, n=5). n.s.: no significant difference**.**

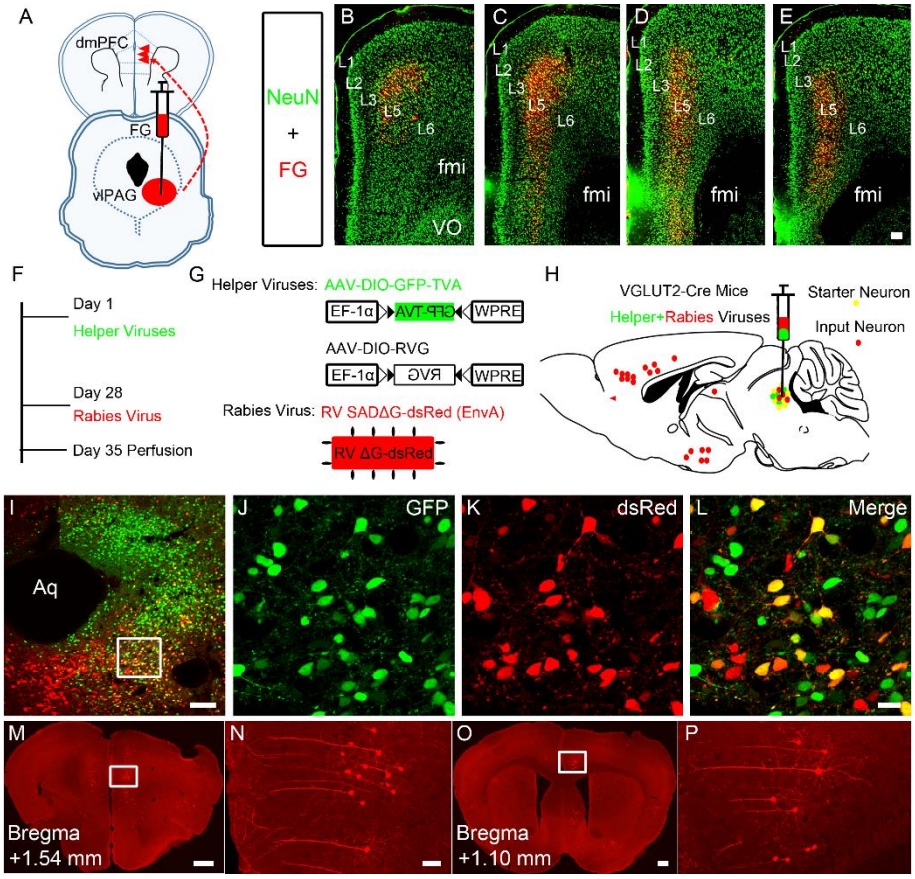

Figure 2. Projections from the dmPFC to the VGLUT2-containing neurons in the vlPAG.

(**A**) Schematic diagram of retrograde tracing projections neurons in dmPFC, which were labeled with FG injected into the vlPAG. (**B**-**E**) In different coronal dmPFC sections, the double staining of FG (red) injected into the vlPAG and NeuN (green). L1-L6: layer 1 to layer 6, fmi: forceps minor of the corpus callosum, VO: ventral orbital cortex. (**F**-**H**) Schematic of rabies-based trans-synaptic tracing. VGLUT2-Cre mice were transduced with two AAVs in the vlPAG followed by EnvA-pseudotyped, glycoprotein (RG)-deleted, and dsRed-expressing rabies virus. VGLUT2 starter cells are labeled in yellow, and presynaptic partners throughout the brain are labeled in red, as shown on a schematic sagittal section of the mouse brain. (**I**-**L**) Coronal sections through the vlPAG of a VGLUT2-Cre tracing brain showing the location of starter cells (yellow), which were double stained with GFP (green) and dsRed (red). The area in the white frame in **I** was magnified in **J**-**L**. Aq: aqueduct (**M**-**P**) A coronal section through the dmPFC and a section through the ACC showing the dsRed labeled presynaptic projection neurons. The areas in the white frames in **M** and **O** were magnified in **N** and **P**. Scale bars=100 μm in **D** (applied in **A**-**C**), 100 μm in **I**, 20 μm in **L** (applied in **J**-**K**), 300 μm in **M**, 50 μm in **N** (applied in **P**), 300 μm in **O**. All experiments were repeated three times and yielded consistent results.

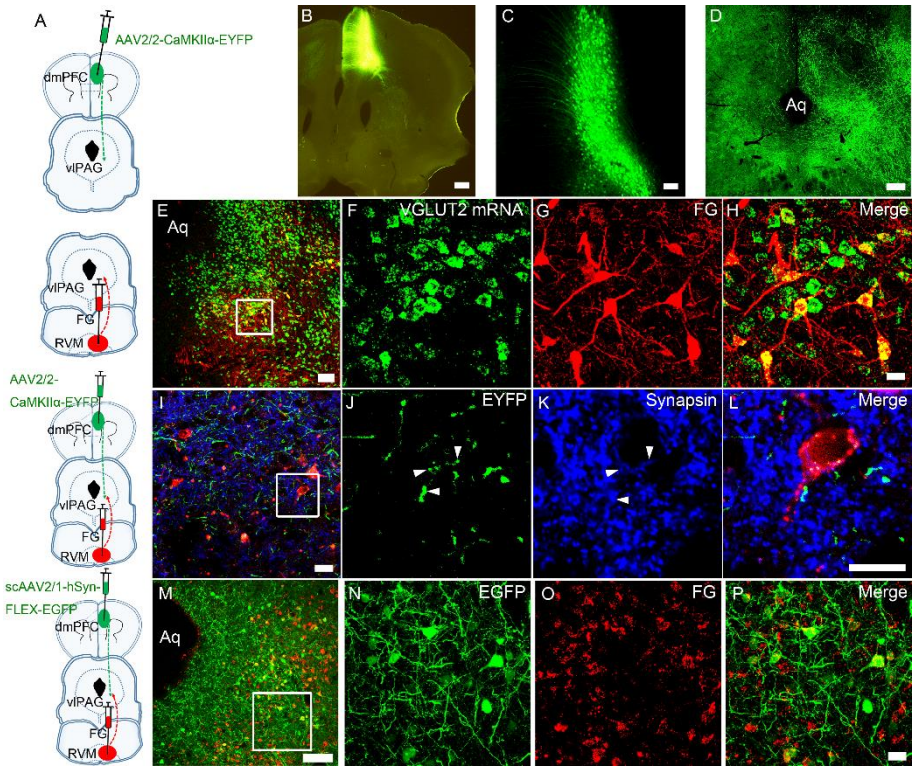

Figure 3. Light microscope observation of the dmPFC-vlPAG-RVM neural pathway.

(**A**) Schematic diagram of the dmPFC-vlPAG-RVM neural pathway by using various kinds of tracers or viruses. (**B-C**) Infection images of AAV2/2-CaMKIIα-EYFP in the dmPFC. (**D**) The distributions of EYFP-labeled fibers coming from the dmPFC pyramidal neurons in the vlPAG. (**E-H**) RVM projection neurons labeled with hybridization signals for VGLUT2 mRNA in the vlPAG. The hybridization signals are visualized with FITC (Green), while FG-ir is visualized with Alexa594 (Red). The area in the white frame in **E** was magnified in **F-H**. (**I-L**) Triple staining of EYFP-labeled fibers (green), FG-ir projection neurons (red), and synapsin-ir terminals (blue) in the vlPAG showing the relationship between fibers projecting from the dmPFC and neurons projecting to the RVM. The area in the white frame in **I** was magnified in **J-L**. The white arrowheads indicate the EFYP-labeled fibers also expressed synapsin and contacted FG-ir projection neurons. **(M-P)** Anterograde trans-synaptic virus EGFP-labeled neurons (green) also expressed FG-ir (red), which indicated the vlPAG-RVM projection neurons received direct innervation by dmPFC. The area in the white frame in **M** was magnified in **N-P**. Scale bars=100 μm in **B**, 50 μm in **C**, 200 μm in **D**, 100

μm in **E**, 10 μm in **H** (applied in **F**-**G**), 100 μm in **I**, 20 μm in **L** (applied in **J**-**K**), 100 μm in **M**, 20 μm in **P** (applied in **N**-**O**). All experiments were repeated three times and yielded consistent results.

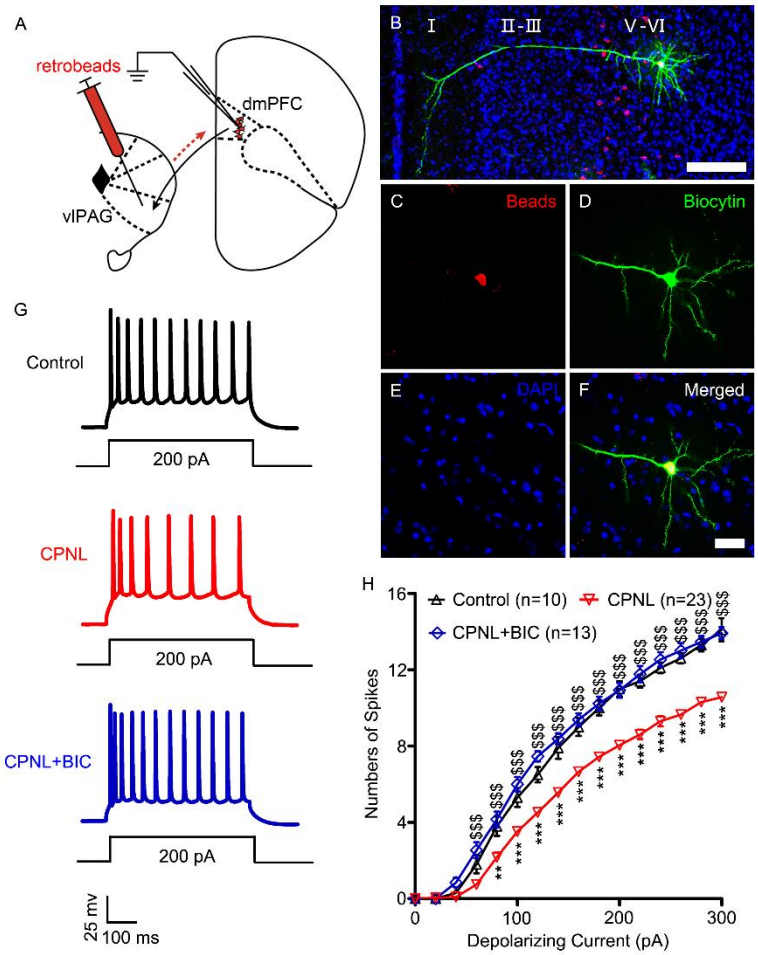

Figure 4. Neuronal activity recorded in dmPFC-vlPAG projection neurons in CPNL and sham mice.

(**A**) Schematic diagram of neurons electrophysiological recording in dmPFC, which were labeled with retrobeads injected into the vlPAG. (**B**-**F**) Triple staining of biocytin-filled neurons (green, indicate recorded neurons), beads-labeled neurons (red, indicate dmPFC-vlPAG projection neurons) and DAPI (blue) in the dmPFC after electrophysiological recording. Scale bar=200 μm in **B**, 50 μm in **F** (applied in **C**-**E**) (**G**) Representative recordings of action potential firing of dmPFC-vlPAG projection neurons in response to current injection (200pA) in control, CPNL, and CPNL+bicuculline groups**.** (**H**) Averaged action potentials of dmPFC-vlPAG projection

neurons induced by step current injections (0-300pA). Note the decrease in excitability of dmPFC-vlPAG projection neurons in CPNL mice and its reversal by bicuculline (BIC, 20 μM). Control group vs CPNL group, $^{**}P<0.005$, $^{***}P<0.001$; CPNL group vs CPNL+BIC group, $^{\$\$\$}P<0.001$; Two-way repeated measures ANOVA with Bonferroni post hoc test.

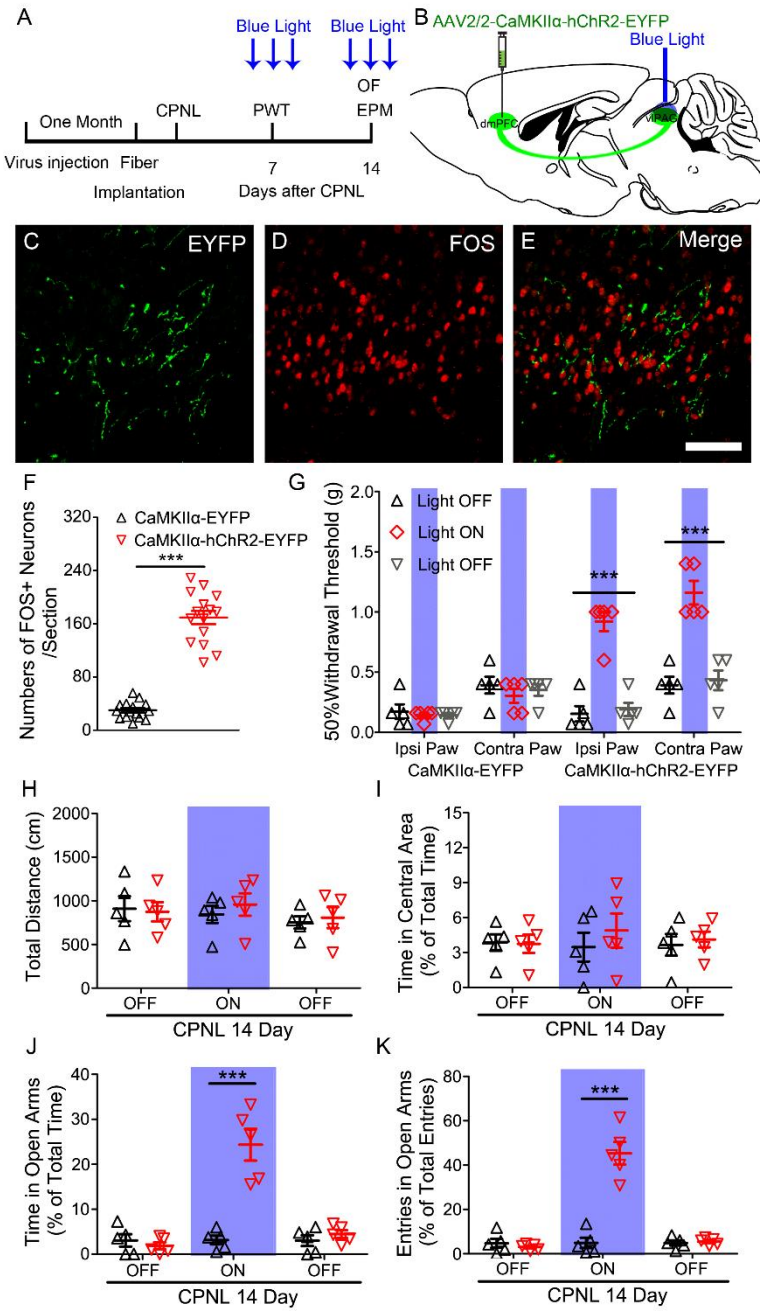

Figure 5. Optogenetic activation of the dmPFC-vlPAG neural pathway attenuated CPNL-induced mechanical hyperalgesia and anxiety-like behaviors.

(**A**-**B**) Representative schematic diagram of optogenetic activation of the dmPFC-vlPAG neural pathway and the procedures for the behavioral testing. (**C**-**E**) Double staining of EYFP-labeled fibers (green) and Fos-ir neurons (red) in the vlPAG after blue light stimulation. Scale bar=50 μm in **E** (applied in **C**-**D**) (**F**) Mean number of Fos-ir neurons in the vlPAG following optogenetic activation (***P<0.001, Student's t-test, n=5 mice per group)**.** (**G**) Mechanical thresholds of the bilateral hindpaws in the CPNL mice after AAV2/2-CaMKIIα-EYFP or AAV2/2-CaMKIIα-hChR2-EYFP virus injection with 473 nm blue light off-on-off stimulation (Ipsilateral, control virus: $F_{(2, 8)}$=0.29, P=0.75; hChR2 virus: F(2, 8)=57.57, P<0.001; Contralateral, control virus: $F_{(2, 8)}$=0.50, P=0.62; hChR2 virus: $F_{(2, 8)}$=42.79, P<0.001; ***P<0.001, one-way repeated measures ANOVA with Turkey's post hoc test, n=5 mice per group). (**H**-**I**) The total distance traveled and percentage of time spent in the central area of the OF test with 3-min light off, 3-min light on and 3-min light off (H: $F_{(1, 16)}$=1.09, P=0.33, t=0.70, P>0.05; I: $F_{(1, 16)}$=0.40, P=0.54, t=0.99, P>0.05; two-way repeated measures ANOVA, with Bonferroni post hoc tests, n=5 mice per group). (**J**-**K**) The percentage of time in and the percentage of entries into the open arms of the EPM test with 3-min light off, 3-min light on and 3-min light off (J: $F_{(1, 16)}$=21.12, P<0.01, t=8.65, P<0.001; K: $F_{(1, 16)}$=47.95, P<0.001, t=11.37, P<0.001; ***P<0.001, two-way repeated measures ANOVA, with Bonferroni post hoc tests, n=5 mice per group).

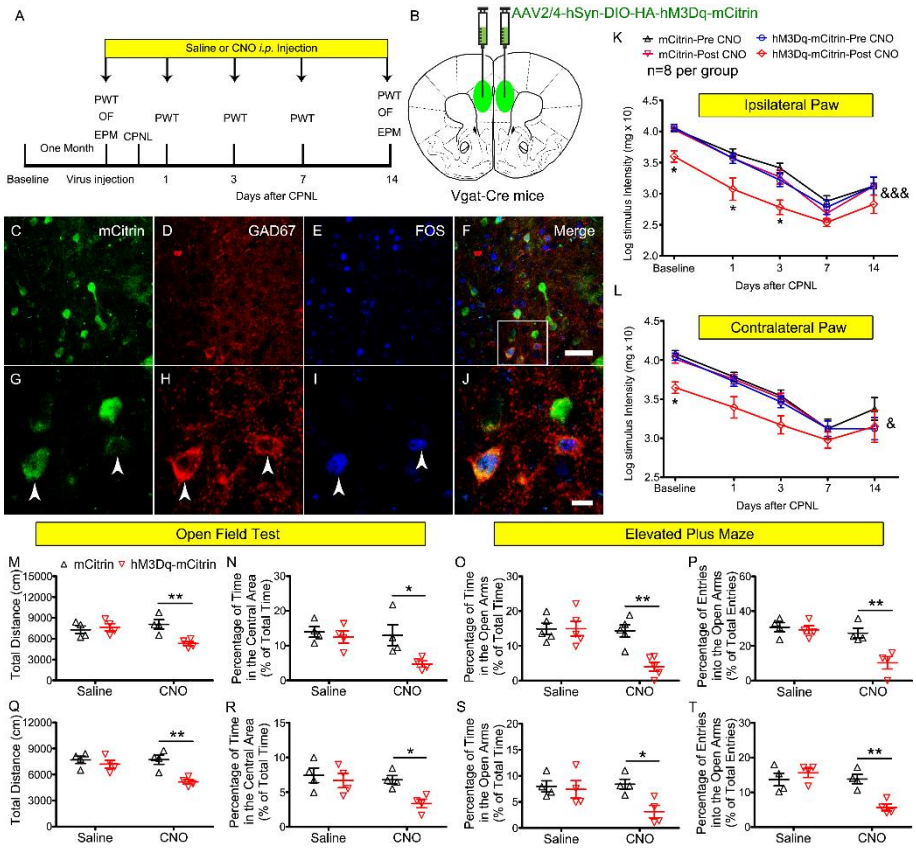

988

989 **Figure 6. Chemogenetic activation of inhibitory neurons in the dmPFC worsens**
990 **CPNL-induced mechanical hyperalgesia and anxiety-like behaviors.**

991 (**A**-**B**) Representative schematic diagram of hM3Dq virus injected into the dmPFC of
992 Vgat-Cre mice and the procedures for the behavioral test. (**C**-**J**) The triple staining of
993 mCitrin (green), GAD67 (red), and FOS (blue) in the dmPFC after CNO *i.p.* injection.
994 The area in the white frame in **F** was magnified in **G**-**J**. The white arrowheads indicate
995 the co-expression of mCitrin, GAD67 and FOS. Scale bars=40 μm in **F** (applied in **C**-
996 **E**), 10 μm in **J** (applied in **G**-**I**) (**K**-**L**) Mechanical thresholds of the bilateral hindpaws
997 following control virus or hM3Dq virus injection and CNO 1 mg/kg *i.p.* injection
998 (hM3Dq virus, Ipsilateral: $F_{(1, 56)}$=19.53, P<0.001; Contralateral: $F_{(1, 56)}$=5.65, P<0.05;
999 control virus, Ipsilateral: $F_{(1, 56)}$=1.46, P=0.24; Contralateral: $F_{(1, 56)}$=1.09, P=0.31;
1000 $^{\&}P$<0.05, $^{\&\&\&}P$<0.001, $^{*}P$<0.05, two-way repeated measures ANOVA, with Bonferroni
1001 post hoc tests, n=8 mice per group). (**M**-**P**) The total distance traveled and percentage
1002 of time in the central area in the OF and the percentage of time in and percentage of
1003 entries into the open arms in the EPM with CNO injection under normal conditions (**M**:
1004 $F_{(1, 12)}$=5.13, P<0.05, t=3.71; N: $F_{(1, 12)}$=6.22, P<0.05, t=2.99; O: $F_{(1, 12)}$=8.85, P<0.01,

t=4.22; **P**: $F_{(1,\ 12)}$=10.55, P<0.01, t=4.22; *P<0.05, **P<0.01, two-way measures ANOVA, with Bonferroni post hoc tests, n=4 mice per group). (**Q**-**T**) The total distance traveled and percentage of time in the central area in the OF and the percentage of time in and percentage of entries into the open arms in the EPM with CNO injection at 14 days post CPNL (**Q**: $F_{(1,\ 12)}$=12.87, P<0.01, t=4.23; R: $F_{(1,\ 12)}$=5.92, P<0.05, t=2.83; S: $F_{(1,\ 12)}$=5.32, P<0.05, t=2.95; **T**: $F_{(1,\ 12)}$=5.05, P<0.05, t=4.14; *P<0.05, **P<0.01, two-way measures ANOVA, with Bonferroni post hoc tests, n=4 mice per group).

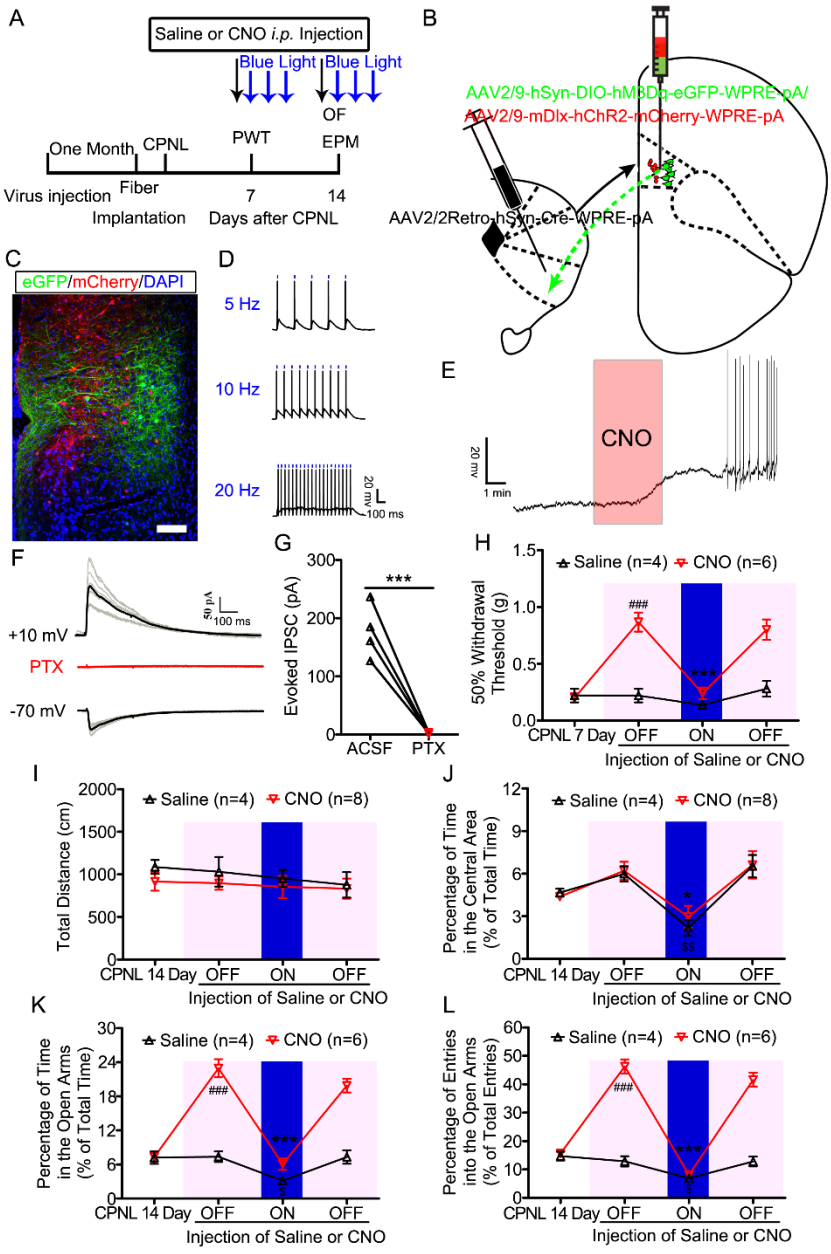

Figure 7. Optogenetic activation of inhibitory neurons in the dmPFC reversed activation of dmPFC-vlPAG pathway-induced analgesic and anxiolytic behaviors. (**A**-**B**) Representative schematic diagram of hChR2 and hM3Dq viruss injected into the dmPFC, retro-Cre virus injected into the vlPAG of C57 mice and the procedures for the behavioral test. (**C**) The triple staining of eGFP (green), mCherry (red), and DAPI (blue) in the dmPFC. Scale bars=100 μm. (**D**) Representative recordings of action potential firing of inhibitory neurons in response to 5 Hz, 10 Hz, and 20 Hz light photostimulation. (**E**) Whole-cell current-clamp recording from an hM3Dq-expressing dmPFC-vlPAG projection neurons. Brief bath application of 40 μM CNO (red box) caused a depolarization and action potential firing. (**F-G**) Sample traces showing that light-evoked eIPSCs in dmPFC-vlPAG projection neurons were blocked by bath application of PTX (***P<0.01, Student's t-test). (**H**) The mechanical threshold of injured hindpaw with CNO injection and blue light stimulation at 7 days post CPNL (CNO, $F_{(3, 15)}$=27.14, P<0.001, ***P<0.01; Saline: $F_{(3, 9)}$=1.03, P=0.426; one-way repeated measures ANOVA, with Tukey post hoc tests; $^{###}P$<0.001, Student's t-test). (**I**-**J**) The total distance traveled and percentage of time in the central area in the OF with CNO injection and blue light stimulation at 14 days post CPNL (**I**: CNO, $F_{(3, 21)}$=2.64, P>0.05; Saline: $F_{(3, 9)}$=1.03, P=0.426; **J**: CNO, $F_{(3, 21)}$=5.25, P<0.01, *P<0.05; Saline: $F_{(3, 9)}$=11.47, P<0.01, $^{\$\$}P$<0.01; one-way repeated measures ANOVA, with Tukey post hoc tests). (**K**-**L**) The percentage of time in and percentage of entries into the open arms in the EPM with CNO injection and blue light stimulation at 14 days post CPNL (**K**: CNO, $F_{(3, 15)}$=55.60, P<0.001, ***P<0.01; Saline: $F_{(3, 9)}$=4.86, P=0.028, $^{\$}P$<0.05; **L**: CNO, $F_{(3, 15)}$=83.05, P<0.001, ***P<0.01; Saline: $F_{(3, 9)}$=6.38, P=0.013, $^{\$}P$<0.05; one-way repeated measures ANOVA, with Tukey post hoc tests; $^{###}P$<0.001, t test).

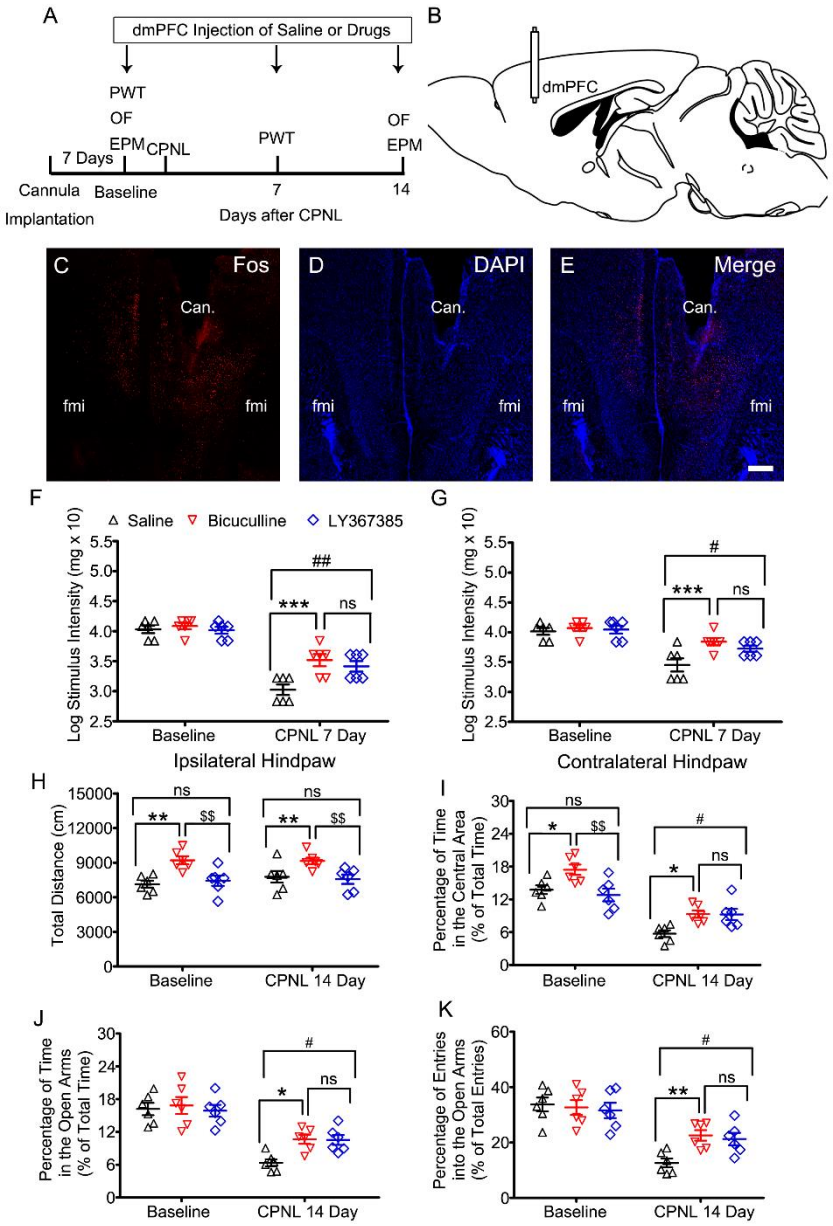

Figure 8. Suppression of GABA$_A$R and mGluR1 in the dmPFC reversed CPNL-induced mechanical hyperalgesia and anxiety-like behaviors.

(**A**-**B**) Representative schematic diagram of cannula placement in the dmPFC and the behavioral testing procedure. (**C**-**E**) Double staining of FOS-ir neurons (red) and DAPI (blue) in the dmPFC after drug infusion. Scale bar=200 μm in **E** (applied in **C**-**D**) Can.: cannula, fmi: forceps minor of the corpus callosum (**F**-**G**) Mechanical thresholds of the bilateral hindpaws following dmPFC injections of saline, bicuculline 0.1 μg or LY 367385 0.4 nmol at baseline and 7 days post CPNL (Ipsilateral, $F_{(2, 15)}$=6.87, P<0.001: baseline t=0.51, t=0.14; CPNL t=4.55, t=4.55; Contralateral, $F_{(2, 15)}$=7.56, P<0.001: baseline t=0.56, t=0.31; CPNL t=3.98, t=3.60; $^{\#}P$<0.05, $^{\#\#}P$<0.01, ***P<0.001, two-

way repeated measures ANOVA, with Bonferroni post hoc tests, n=6 mice per group). (**H**-**I**) The total distance traveled and percentage of time in the central area in the OF following dmPFC injection of saline, bicuculline or LY 367385 at baseline and 14 days post CPNL (total distance, $F_{(2, 15)}$=10.60, P<0.01: baseline t=3.79, t=0.55; CPNL t=2.85, t=0.38; time percentage in the central area, $F_{(2, 15)}$=6.56, P<0.01: baseline t=2.91, t=0.77; CPNL t=2.52, t=2.80; $^{\#}P$<0.05, *P<0.05, **P<0.01, $^{\$\$}P$<0.01, two-way repeated measures ANOVA, with Bonferroni post hoc tests, n=6 mice per group). (**J**-**K**) The percentage of time in and percentage of entries into the open arms in the EPM following dmPFC injection of saline, bicuculline or LY 367385 at baseline and 14 days post CPNL (time percentage in the open arms, $F_{(2, 15)}$=2.96, P>0.05: baseline t=0.43, t=0.21; CPNL t=2.86, t=2.78; entries percentage in the open arms, $F_{(2, 15)}$=2.35, P>0.05: baseline t=0.33, t=0.66; CPNL t=3.04, t=2.64; $^{\#}P$<0.05, *P<0.05, **P<0.01, two-way repeated measures ANOVA, with Bonferroni post hoc tests, n=6 mice per group). n.s.: no significant difference**.**